

# Optical Fiber Based Temperature Sensors: A Review

Rahul Kumar Gangwar <sup>1</sup>, Sneha Kumari <sup>2,\*</sup>, Akhilesh Kumar Pathak <sup>3,\*</sup>, Sai Dheeraj Gutlapalli <sup>4</sup>  
and Mahesh Chand Meena <sup>1</sup>

- <sup>1</sup> Department of Physics & Electronics, Rajdhani College, University of Delhi, New Delhi 110015, India  
<sup>2</sup> Centre for Nanoscience and Engineering (CeNSE), Indian Institute of Science, Bangalore 560012, India  
<sup>3</sup> Center for Smart Structures and Materials, Department of Mechanical Engineering, Northwestern University, Evanston, IL 60208, USA  
<sup>4</sup> Department of Internal Medicine, Richmond University Medical Center, Staten Island, NY 10310, USA  
\* Correspondence: snehakumari@iisc.ac.in (S.K.); akhilesh.pathak@northwestern.edu (A.K.P.)

**Abstract:** The current generation is witnessing a huge interest in optical waveguides due to their salient features: they are of low cost, immune to electromagnetic interference, easy to multiplex, have a compact size, etc. These features of optical fibers make them a useful tool for various sensing applications including in medicine, automotives, biotechnology, food quality control, aerospace, physical and chemical monitoring. Among all the reported applications, optical waveguides have been widely exploited to measure the physical and chemical variations in the surrounding environment. Optical fiber-based temperature sensors have played a crucial role in this decade to detect high fever and tackle COVID-19-like pandemics. Recognizing the major developments in the field of optical fibers, this article provides recent progress in temperature sensors utilizing several sensing configurations including conventional fiber, photonic crystal fiber, and Bragg grating fibers. Additionally, this article also highlights the advantages, limitations, and future possibilities in this area.

**Keywords:** waveguide; photonic crystal; optical fiber; Bragg gratings; temperature; sensor; COVID-19



**Citation:** Gangwar, R.K.; Kumari, S.; Pathak, A.K.; Gutlapalli, S.D.; Meena, M.C. Optical Fiber Based Temperature Sensors: A Review. *Optics* **2023**, *4*, 171–197. <https://doi.org/10.3390/opt4010013>

Academic Editor: Marco Gandolfi

Received: 29 January 2023

Revised: 15 February 2023

Accepted: 20 February 2023

Published: 23 February 2023



**Copyright:** © 2023 by the authors. Licensee MDPI, Basel, Switzerland. This article is an open access article distributed under the terms and conditions of the Creative Commons Attribution (CC BY) license (<https://creativecommons.org/licenses/by/4.0/>).

## 1. Introduction

Reliable temperature monitoring plays a key role in the metallurgical industry, the aerospace field, nuclear energy production, and medical applications [1,2]. In the metallurgical industry, real-time monitoring of the internal temperature of high-temperature boilers is key to measuring combustion efficiency and safety prevention [3,4]. On the other hand, temperature monitoring inside the turbines and combustion chambers of an aero-engine or aircraft can help extend its service life [5–7]. Recently, the appearance of COVID-19 gained huge interest in terms of the need for temperature-monitoring instruments in the medical sector for continuous monitoring of the temperature of individuals in public places [8,9].

According to the accuracy, detection, and installation techniques, high-temperature-monitoring technology can be categorized as (i) contact measurement [10], and (ii) non-contact measurement [11]. Thermocouple sensors made of expensive metals are generally utilized for the former type of temperature sensing due to their ease of operation, mature preparation approach, and wide operating range [12]. However, thermocouple sensors suffer several limitations—they have a short life, poor corrosion resistance, low accuracy, are susceptible to electromagnetic interferences, etc. The main concerns when using thermocouple devices are that their metal or alloys used during fabrication which can be easily oxidized and damaged at high temperatures, leading to a shorter service life and poor sensing accuracy [13]. Infrared thermography is a type of non-contact temperature-sensing technology, designed to avoid direct contact between the sensing equipment and high-temperature environments to provide a non-destructive sensing performance [14]. Unfortunately, the radiation temperature-monitoring technology is only suitable for surface measurements, i.e., explosion flame, and cannot detect the temperature of the internal

structure of the closure device. Extremely harsh environments with high pressures, high temperatures, and strong electromagnetic radiation present a challenge to these conventional detection techniques.

Compared to conventional sensing technology, optical fiber-based sensors have gained huge interest owing to their excellent properties: they are of low cost, immune to electromagnetic interference, easy to multiplex, have a compact size, etc. [15]. To date, several approaches have already been implemented for temperature sensing including microstructured optical fibers (MOFs) [16,17], conventional fibers (e.g., single-mode fibers (SMFs), multimode fibers (MMFs), and plastic optical fibers (POF)) [18–21], and grating-based fibers (e.g., fiber Bragg grating (FBG), long period grating (LPG), and tilted FBG (TFBG)) [22]. The commonly employed high-temperature-sensing optical fibers mainly include silica and MOFs. Theoretically, the maximum temperature that a temperature sensor can detect is based on the fiber materials rather than that of its sensing mechanism. Usually, silica-fiber-based temperature sensors are limited to operating within 1000 °C due to the diffusion of the germanium dopant [1]. Additionally, temperature sensors based on pure silicon fibers such as MOFs can operate at 1300 °C, which is closer to the melting point of silicon, whereas temperature sensors based on single-crystal fibers can operate stably below 1900 °C. Figure 1 summarizes all types of optical fiber temperature sensors.

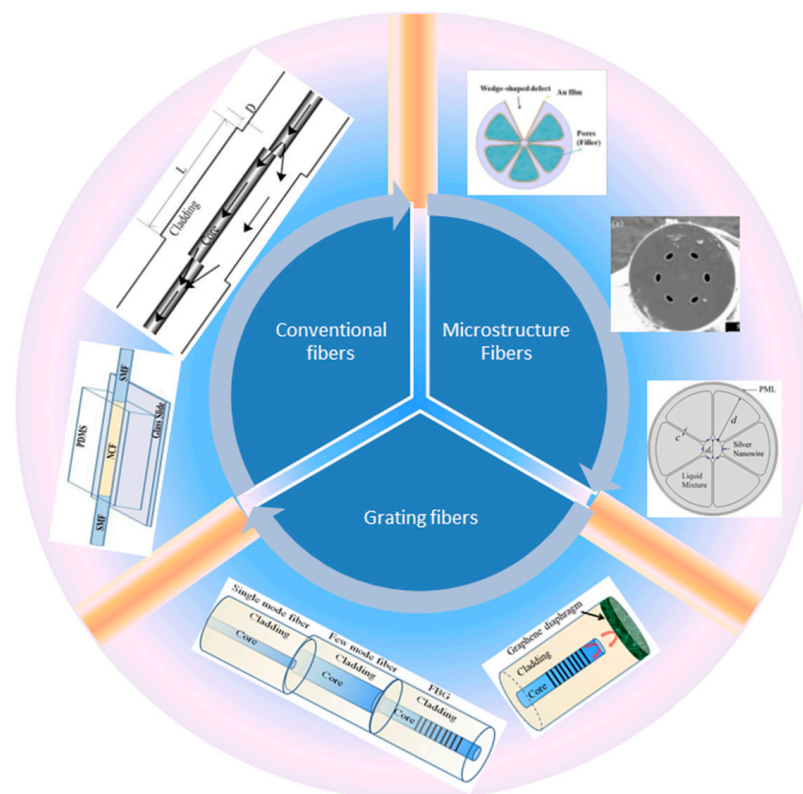


**Figure 1.** Summary of various optical fiber-based temperature sensors.

In this article, we have reviewed several optical fiber-based temperature sensors reported in recent decades, including their design, fabrication, sensing materials, and performance. This review is organized in the following manner: Section 2 provides a brief survey of microstructure optical fibers along with the advancement in the technology; Section 3 covers the conventional optical fibers and their application in temperature sensing; Section 4 comprises Bragg grating-based fibers and their role in temperature sensing; and Section 5 provides a brief description of future prospects and challenges. Finally, the overall conclusion is drawn in Section 6.

## 2. Microstructure Optical Fibers (MOFs)

The last decade has witnessed an enormous interest in optical fibers used for sensing and long-distance operation applications [23–25]. The optical fiber in sensors is applied as a sensing element to monitor surrounding parameters such as strain, pressure, vibration, and temperature. Among conventional fibers, MOFs have played a key role in various sensing applications [26–28]. MOFs are waveguides made of optical fibers in which the guiding property is acquired by modifying the waveguide structure rather than the waveguide's index of refraction [29]. Light is steered using complete internal reflection in ordinary optical fibers. A core with a refractive index greater than that of the surrounding material is where the guiding takes place (cladding). The cladding and core can be doped differently, or various materials can be used, to produce the index change [30]. The method used in microstructured fibers is fundamentally different. Fibers are made of a single substance (often silica), and light directing is accomplished by the existence of air gaps in the region around the solid core [31]. Unlike conventional optical fibers, photonic crystal fibers (PCFs) are made up of small air holes that are spaced at regular intervals, enabling greater design freedom and unique optical properties [32,33]. A periodic pattern of air holes extending the full length of a PCF, centered on a solid or hollow core, is what gives this geometry its name. The primary distinction between the two types of fibers is based on the fact that PCF waveguide properties derive from an arrangement of extremely small and closely spaced air holes rather than from the spatially varying glass composition of a conventional optical fiber, which runs the entire length of the fiber.

Based on post-processing techniques, the micro air holes can also be filled with liquid, gas, or even solid materials, greatly changing the PCF guiding characteristics and enabling the fabrication of a variety of functional fiber devices such as electrically controlled optical switches [34–36], all-optical modulators [37], temperature-controlled tunable optical filters [38], photonic bandgap fiber polarimeters [39,40], and PCF sensors [41]. In this section, the current status of research on MOF-based temperature sensors is discussed.

Micro-optical devices have been quickly developed in recent years as a result of technological advancements in micro-fiber manufacturing [42,43], particularly in the field of dynamic temperature monitoring [44]. A number of significant efforts have been made to improve the sensitivity and reliability of the proposed optical fiber-based temperature sensors, including micron-scale processing of couplers and ring resonators [45,46], selective liquid infiltration of high birefringence photonic crystal fibers (HBPCFs) [47,48] and filled PCFs [49,50]. Most temperature sensors based on classic fiber constructions with silica backgrounds have a temperature sensitivity less than  $0.3 \text{ nm}/^\circ\text{C}$  [51], which is primarily constrained by the modest thermo-optical coefficient difference between the fiber core and cladding. To circumvent these constraints, Qian et al. suggested a PCF-based temperature sensor that gives an extremely high sensitivity of  $6.6 \text{ nm}/^\circ\text{C}$  by selectively infiltrating a thermosensitive liquid, such as alcohol, in the air holes to increase the thermo-optic coefficient [49]. In this experiment, the fiber loop mirror of alcohol-filled highly birefringence PCFs is placed in a temperature-controlled container for investigating the temperature characteristics of the proposed sensing device. Figure 2 shows the experimental setup for the temperature measurement and the inset of Figure 2 shows the cross-section of the high birefringence PCF provided. Dora et al. suggested a temperature-sensitive device based on nematic liquid crystal-filled PCFs, with a temperature sensitivity of  $3.90 \text{ nm}/^\circ\text{C}$  [52]. The PCF is still made up of a high-index solid silica core encircled by a lower index cladding even after liquid ethanol has been introduced into the holes by capillary force and air pressure (since ethanol's index is lower than silica's). Total internal reflection in the higher index core therefore directs light via this fiber, and temperature variations allow for constant adjustment of the index of the ethanol within the holes (which changes the propagation modes of the PCF such as the mode index and confinement loss).

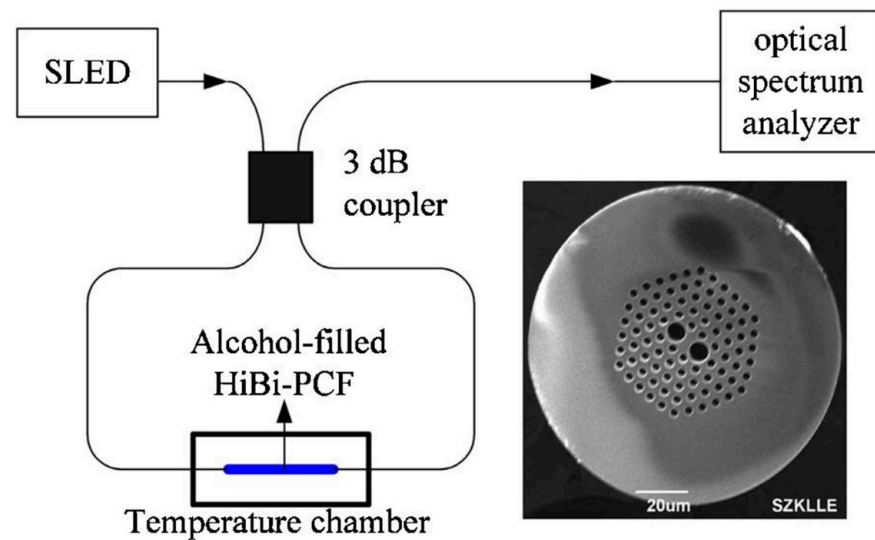


**Figure 2.** Experimental setup for a temperature sensor based on an FLM. Inset: SEM of the used HiBi-PCF [reprinted with permission from [49] © The Optical Society].

Due to its strong thermal resistance and immunity to electromagnetic noise and corrosion, fiber sensors are likely the only option for sensing at temperatures above 800 °C. In 2013, Chen et al. described for the first time a truly distributed pressure sensing at room and very high temperature sensing by utilizing a pressure-sensitive fibers. This was based on an optical frequency domain reflectometry measurement of Rayleigh scattering in a fiber. This technique has been used to provide a distributed sensing solution for measurements of temperature, axial strain, and transverse stress. Air-hole microstructural fibers are employed to broaden their applicability for pressure sensing at high temperatures. Temperatures ranging from 24 to 800 °C are used to detect pressure distributions of up to 13.8 MPa (2000 psi) [53]. Another method for measuring temperature is to utilize Fabry–Pérot interferometers (FPIs). Because of their sensitivity, extremely tiny size, easy design, and versatility in modifying sensitivity and dynamic range, FPIs are a common sensor arrangement. FPIs may be improved as remote, reliable interferometric multiparameter sensors by using an optical fiber configuration. The FPI connected to an optical fiber can be configured in two different ways. An extrinsic FPI uses two reflector surfaces or etalon put outside the fiber, whereas an intrinsic FPI uses two reflectors built inside the fiber. A supporting structure with an intrinsic FPI creates an air cavity. It is possible to use these air cavities as high-reflecting mirrors. Consequently, the extrinsic structure is helpful in obtaining a good interference signal pattern. A microstructure temperature sensor can be wavelength and frequency encoded at the same time presented by Li et al. [54]. In this work, the sensor system has the potential for over 1000 multiplexing capacity via a single fiber with the hybrid frequency-division-multiplexing/wavelength-division-multiplexing (FDM/WDM) method. A temperature sensitivity of approximately 7.91 pm/°C is established experimentally using quasi-distributed measurement of temperature change. Tan et al. presented a work which shows how to make an intrinsic FPI sensor for high temperature detection with high fringe contrast by splicing a short piece of microstructured fiber to a single-mode fiber [55]. The two strands of the microstructured fiber are spliced together using the conventional arc-discharge process. The interference spectrum's fringe contrast can approach 20 dB. There is theoretical study and thermal testing up to 1000 °C. Monitoring the dip wavelength shift yields a temperature sensitivity of 17.7 pm/°C. This suggested sensor is small and has a significant potential for high temperature-sensing applications using simply splicing and cleaving techniques.

Using two mirrors and beam splitters, the earliest conventional Mach–Zehnder interferometers (MZIs) featured two independent arms, the reference arm and the sensing arm. When this happens, an optical fiber is used in its stead to avoid the cumbersome and

intricately aligned traditional setup. Two different kinds of MZIs are readily available: (i) a modal interferometer, and (ii) a two-arm interferometer. A two-arm MZI needs a long optical fiber, one or two couplers, and involves splitting and recombining two monochromatic optical beams that travel in distinct fibers. The optical path difference (OPD) between the two arms determines the interference component of the recombined light.

To metallize a fiber surface in a typical fiber-based sensor, first strip the fiber jacket and then physically or chemically remove the fiber cladding, nearly to the core, to permit evanescent coupling with a plasmon mode. The associated operations directly raise the overall fabrication cost and jeopardize device dependability. The rapid creation of a novel form of PCF with an array of air holes along the propagation direction has piqued the curiosity of researchers worldwide in recent years. Many studies sought to insert metallic layers or rods into PCFs and were successful in containing the plasmonic modes within the fiber [56–58]. Metallization of PCFs can be accomplished using stack and draw [59] or by pumping molten metal into the hollow channels of silica glass PCFs [57]. Metal layers can be deposited in the side of the PCF using either a high pressure chemical vapour deposition (CVD) approach [59] or a wet chemistry deposition process employed in the manufacture of metal-covered hollow waveguides [60]. In 2013, Favero et al. experimentally demonstrated a PCF made of a specially doped germanium core as shown in Figure 3a [61]. This was a PCF with a germanium core sandwiched between two single-mode fibers to form an interferometer for the temperature measurement. The experimental set for the temperature detection is shown in Figure 3b. One end of the fiber was deposited with the gold film in order to work in the reflection mode. The proposed device shows very high temperature dependence with a sensitivity of 78 pm/°C.

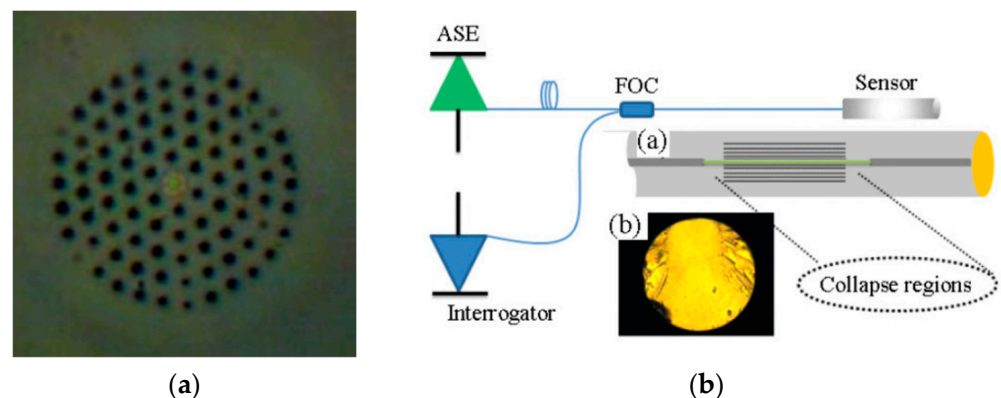


**Figure 3.** (a) cross-section of the microstructure fiber and (b) experimental setup with collapsed region of the microstructure fiber and gold coated at the one end of the single-mode fiber [61].

By inserting a silver nanowire into the holes of a six-hole PCF, a temperature sensor was designed based on the surface plasmon resonance effect [62]. The cross-sectional area of the proposed sensing device is shown in Figure 4a and different air holes coated with silver nanowires and filled with the high thermo-optic coefficient liquid, a mixture of ethanol and chloroform are shown in Figure 4b. As a sensing medium, a liquid combination (ethanol and chloroform) with a high thermo-optic coefficient is injected into the PCF holes. The filled silver nanowires can sustain resonance peaks, and the peak will move when temperature changes cause changes in the mixture's refractive indices. The temperature change may be observed by monitoring the peak shift. Because the refractive index of the filled mixture is near to that of the PCF material, the resonance peak is particularly temperature sensitive. Our numerical results show that a temperature sensitivity of up to 4 nm/K is possible.

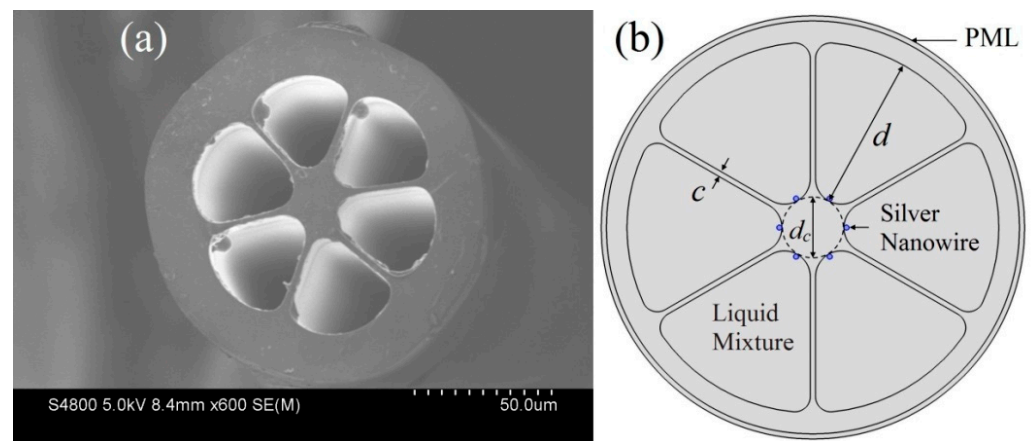


**Figure 4.** (a) Cross-section of the six-hole PCF; (b) schematic of the proposed sensing device coated with silver nano wires and filled with the mixture of ethanol and chloroform [62].

A sensing device with improved sensitivity based on the MOF and worked on the surface plasmon resonance principle was further demonstrated by the same group in 2014 [63]. The MOF's air holes are coated with silver metal and filled with a mixture of ethanol and chloroform which have a very high thermo-optic coefficient. The usage of all six fiber openings, as well as their relatively large size, should make silver coating and liquid mixture filling easier. Temperature fluctuations will cause changes in the coupling efficiency between the core-guided mode and the plasmonic mode, resulting in various loss spectra being recorded. The liquid mixture's refractive index is near to that of the MOF material, which improves coupling efficiency and sensitivity. Numerical results depict a temperature sensitivity of 5.6 nm/K and that the most sensitive range of the sensor can be modified by varying the volume ratios of ethanol and chloroform. Apart from these structures, different temperature-sensing devices with a different configurations of the MOF are demonstrated [64–67]. In 2015, Scarcia et al. proposed an accurate theoretical analysis of the viability of a unique fiber-optic temperature sensor designed as a standalone device [68]. The sensor is built on a trio of integrated/spliced microstructured optical fibers (MOFs). The first incorporates an appropriate cascade of LPGs into the core. The other two sensor parts are a single-mode intermediate MOF and a ytterbium-doped MOF laser. The three MOFs are made to be readily spliced together, as shown in Figure 5. The entire design is carried out using ad hoc computer code created specifically for this purpose. A low-cost pump diode laser at 980 nm wavelength and a commercial optical power detector are all that is required for a comprehensive temperature-monitoring setup. The simulated sensitivity  $S = 315.1 \mu\text{W}/^\circ\text{C}$  and operation range  $\Delta T = 100^\circ\text{C}$  are adequate for real-world applications [68]. In 2015, two all-fiber loop mirrors employing a clover microstructured fiber for simultaneous temperature and strain monitoring are demonstrated [69]. The design of the fiber allowed for the observation of various interferences caused by the microstructured fiber core section. Different sensitivities to temperature and strain were obtained, and both physical characteristics may be discriminated using a matrix technique. For temperature and strain, resolutions of  $\pm 2^\circ\text{C}$  and  $\pm 11 \mu\epsilon$  for the first structure and  $\pm 2.3^\circ\text{C}$  and  $\pm 18 \mu\epsilon$  for the second were obtained.

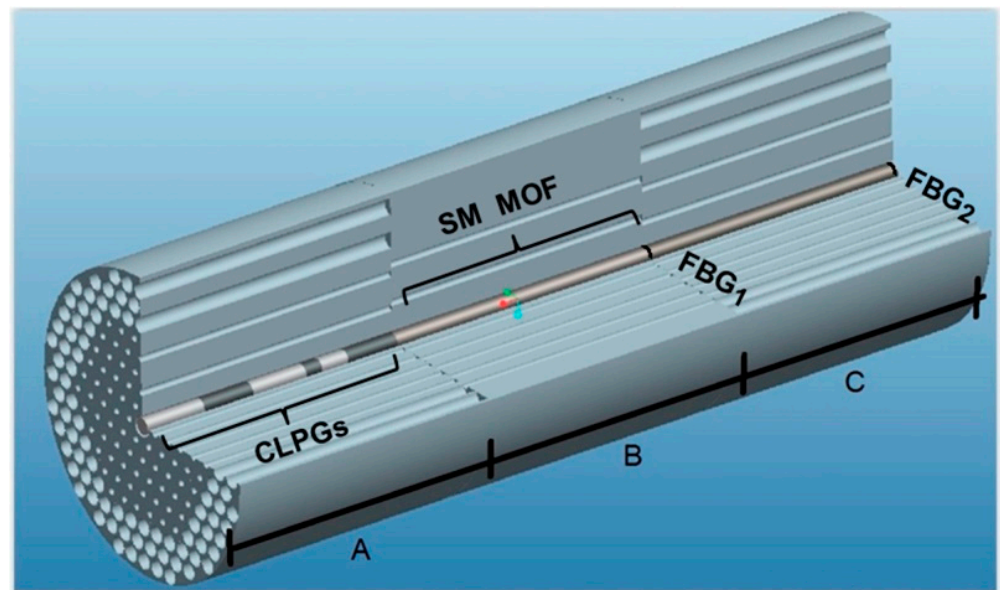


**Figure 5.** Cross-section of the proposed temperature sensor [68].

A wide variety of the MOF-based temperature sensors have been developed by using different configurations and sensing techniques [67,70–75]. In 2016, the use of femtosecond laser ablation to etch fiber Bragg gratings into the core of pure silica suspended-core microstructured optical fiber (SCFs) was reported [76]. Because the concentrated femtosecond laser beam is not greatly deformed when traveling through the fiber cladding, the SCF's basic shape (three big holes) enables for direct writing of FBGs. These can withstand temperatures of up to 1300 °C and can be wavelength divided multiplexed. Temperature sensing up to 1100 °C was achieved by measuring the interference spectrum's fringe changes as the temperature varied [77]. The sensor head in this study is constructed by splicing a single-mode fiber (SMF) with a suspended core microstructured optical fiber (SCF), resulting in an SMF–2SCF–SMF configuration since the reflected light travels twice the physical length of the SCF. Because the SCF is a single-material device, extremely high temperatures may be measured, while the sensor head's all-splice simplicity results in a low-cost and steady operation.

In optical fiber-based Sagnac interferometer, a 3 dB fiber coupler splits the incoming light into two directions before combining the two counter-propagating beams at the same coupler. The polarization-dependent mode propagation speed that is led along the loop serves as a proxy for the optical path difference. In 2017, a very sensitive temperature sensor based on an all-fiber Sagnac loop interferometer and a metal-filled side-hole PCF was demonstrated [45]. An extremely high sensitivity of  $-9.0 \text{ nm}/^\circ\text{C}$  was observed using the indium-filled side-hole PCF.

An optical fiber is utilized in place of the prism to create a fiber-based SPR sensor. The unclad core is then covered with a metal layer after a tiny segment of the fiber, ideally from the middle, has had its cladding removed. The analyte is further encircled by the metal layer. When the directed rays' evanescent field coincides with the surface plasmon wave vector at the metal–analyte interface, the surface plasmon wave will be excited, which causes a dramatic drop in the power reflectivity spectrum. The external environment parameters such as refractive index, temperature, and the pressure of the analyte had a significant impact on the dip's form; therefore, the SPR fiber sensor may be used for analyte detection in the same way as the prism-based SPR sensor.

PCFs with two side holes filled with metal provide a structure that may be adjusted to modify the birefringence of the fiber by expanding the filler metal. To investigate the influence of filler metal on the temperature sensitivity of the fiber-optic temperature sensor, bismuth, and indium were utilized. Measurements revealed that the indium-filled side-hole

PCF could obtain a very high temperature sensitivity of  $9.0 \text{ nm}/^\circ\text{C}$ . A unique MOF based on side-polished fiber (SPF) was presented in [78] for the temperature-sensing application. Polystyrene microspheres were self-assembled onto the side-polished surface of SPF to generate the microstructure fiber's colloidal crystal coating. Three primary troughs were identified in the transmission spectrum due to the Bragg reflection of the colloidal crystals coating and the strong interaction between the evanescent field and colloidal crystal. The valley modulation amplitude was reported to reach up to 12 dB. Furthermore, the transmission valley demonstrated strong temperature sensitivity. Transmission optical power exhibited a temperature sensitivity of  $0.487 \text{ dB}/^\circ\text{C}$ . A brief description of the different sensing structures and mechanisms was also further explained in 2017 [79].

Using the optimal polymer optical fiber for Bragg grating sensing, fabrication, and analysis of an infinitely single-mode microstructured polymer optical fiber is presented in [80]. This fiber is constructed of cyclo-olefin homopolymer Zeonex grade 480R, which showed a very high glass transition temperature of  $138^\circ\text{C}$  and was not observed to be affected by humidity. The temperature sensitivity of this fiber was obtained of  $24.01 \pm 0.1 \text{ pm}/^\circ\text{C}$  for both increasing and decreasing temperatures. Apart from these sensing devices for temperature measurement, many researchers used MOFs for the simultaneous measurements of two or more physical parameters [81–83]. In 2018, Korganbayev et al. demonstrated a linearly chirped Bragg grating fiber engraved in a microstructured polymer optical fiber for temperature detection during thermal treatments [84]. A KrF laser and uniform phase mask were used to inscribe a CFBG of 10 mm length and 0.98 nm bandwidth in an mPOF fiber. The temperature sensitivity of the CFBG was reported to be  $191.4 \text{ pm}/^\circ\text{C}$ . A novel sensing approach based on a C-type microstructured fiber for simultaneous monitoring of seawater temperature and salinity was presented by Zhao et al. [85]. The C-type fiber structure, as shown in Figure 6, was created by removing the outer wall of one pore from a six-hole microstructured fiber, enabling birefringence to enter and breaking the original pattern of degeneracy. Furthermore, a gold layer was applied to the structure's surface to improve sensing sensitivity using the SPR phenomena. Model studies demonstrated that the suggested filling structure might generate two SPR loss valleys with distinct sensitivity to temperature and salinity. Maximum temperature sensitivity of  $7.609 \text{ nm}/^\circ\text{C}$  was obtained for Y polarization, demonstrating that the designed scheme could not only solve the cross-sensitivity problem of two parameters but also achieve high sensitivity.

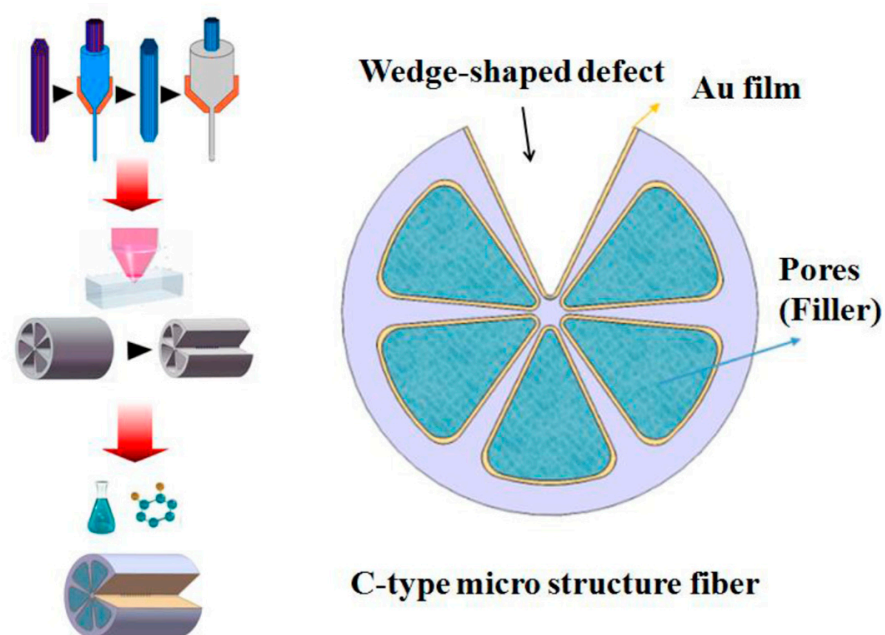


Figure 6. Cross-section of the proposed temperature-sensing device [85].

In recent years, the use of MOFs with different configurations has attracted much attention from researchers [86–88]. In 2019, Su et al. proposed a high-temperature sensor which was based on the suspended-core microstructure optical fiber (SCMF) [89]. The sensor was fabricated by fusing a portion of SCMF between two portions of the multimode fiber (MMF). This kind of configuration allowed multimode interference by the air cladding modes and the core modes in the SCMF. The transmission spectra of the MMF–SCMF–MMF structure were filtered using Fast Fourier transform. The wavelength shift of the main spatial frequency was measured when the temperature varied between 50 and 800 degrees Celsius. Sensitivities of 31.6 and 51.6 pm/°C were reported for the temperature ranges from 50 to 450 °C and 450 to 800 °C, respectively. By using the FPI, in 2019, Zhao et al. experimentally demonstrated composite cavity fiber tip for high temperature sensing [90]. An air cavity and a silica cavity were made of the composite cavity. An oval air hole was introduced in the SMF which serves as the air cavity, enabling FPIs. A small segment of the SMF cascaded to the air cavity to form the silica cavity. The composite cavity fiber tip (CCFT) was effectively encased by a tapered-shaped silica capillary to eliminate the effects of other external physical characteristics (refractive index, humidity, etc.) on the CCFT-FPI. The packed CCFT-FPIs were used for high temperature sensing in the 100–800 °C range. The silica cavity showed a temperature sensitivity of 14.31 pm/°C.

The finite element approach was used to examine a temperature sensor based on a Sagnac interferometer and a liquid crystal-filled microstructured optical fiber [91]. Near the core of the fiber, six submicron liquid crystal columns were added whose refractive index was slightly greater than the silica. In this configuration, the power of the fundamental core modes remained restricted to the silica core, and the mode field properties were heavily impacted by the six submicron liquid crystal columns. The temperature-sensing property of the resultant liquid crystal-filled microstructured optical fiber in the range of 265–325 K was examined using a Sagnac interferometer based on the thermo-optic effect. The temperature sensitivity was 6.23 nm/K with high linearity in the region of 265–295 K. Zhao et al. demonstrated a Sagnac interferometer temperature sensor based on the glycerin-filled MOF [92]. Here, the photosensitive substance was a glycerin solution which is filled in a polarization-maintaining photonic crystal fiber (PMPCF). According to the finite element approach, the temperature sensor had the maximum sensitivity when the PMPCF was filled with a 70% mass fraction of glycerin solution. A linear fit was built between the dip wavelength and the temperature in the experiment, with the temperature rising from –25 to 85 °C in 5 °C steps. The findings showed that the suggested sensor had the greatest temperature sensitivity of 1.5005 nm/°C within the temperature range of –25 to 85 °C.

In another work, the finite element approach has suggested a very sensitive temperature sensor for magnetic fluid (ethanol) utilizing a ring-core-based microstructured optical fiber (MOF) with two huge elliptical air holes alongside the ring core [93]. To boost the ring core's high sensitivity responsiveness, highly sensitive magnetic fluid ethanol is introduced. For the broad working wavelength range of 6500–7000 nm, temperature range of 10–60 °C and applied magnetic field strength range of 50–200 Oe, the highest sensitivity response of 25,641.025 nm/RIU and 10 nm/°C was reported. Here, the sensing device simultaneously measured three different physical parameters. In 2020, an investigation was carried out for a temperature sensor based on the modes coupling effect in a liquid crystal-filled MOF [94]. A full-vectorial finite-element technique (FV-FEM) with completely matched layer and scattering boundary conditions was used to study the sensing properties. Liquid crystal E7 was developed to be infiltrated into one cladding air hole in a PCF to generate a defected core for temperature sensing. As the phase matching requirement was achieved, the core modes coupled to a variety of ordered defect core modes, resulted in a significant rise in the confinement loss spectrum. In 2021, Zheng et al. experimentally demonstrated a temperature sensor based on the Yb-doped silica microstructured optical fibers [95]. In this work, the authors described a unique method for producing Yb-doped silica microstructured optical fibers and its application in high-temperature optical fiber sensing. The Yb-doped silica micro structured optical fiber preforms were made out of

Yb-doped silica core rods (0.1 wt%  $\text{Yb}_2\text{O}_3$ ) and holey pure silica claddings created using UV-curable tube molding and digital light processing 3D printing techniques, respectively. The rod-in-tube approach was used to draw silica preforms to Yb-doped silica microstructured optical fibers without causing significant deformation. Doped microstructured fibers were used in high-temperature sensing ranging from 296.15 to 653.15 K. Figure 7a depicts the scanning microscopic image of the fabricated Yb-doped silica microstructured optical fibers and the refractive index profile of this MOF is shown in Figure 7b. Figure 7c,d depicts the attenuation spectrum and absorption loss of the proposed MOF-based sensing device. The experimental results showed that the proposed sensing device reached a maximum value of temperature sensitivity and a relative temperature sensitivity of 0.0023 K at 348 K and 0.8%/K at 296 K, respectively.

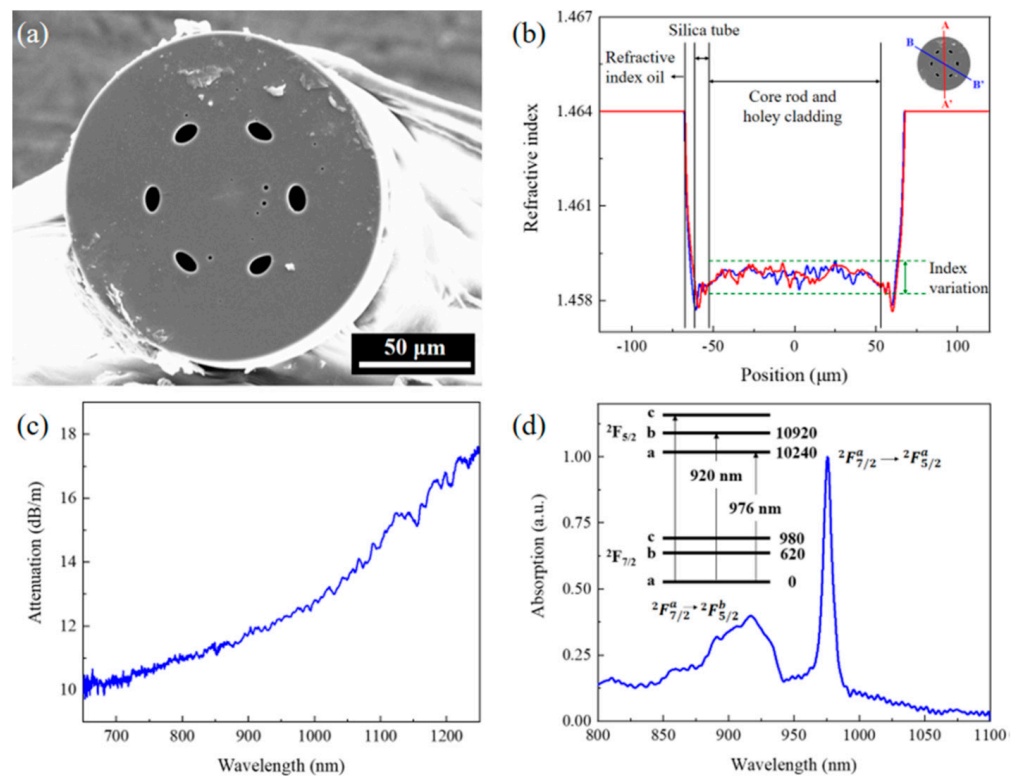


**Figure 7.** (a) SEM image of the Yb-doped silica microstructured optical fiber; (b) the refractive index profile of the fabricated Yb-doped silica microstructured optical fiber along different directions, (c) variation of attenuation of the fiber with different wavelengths, and (d) the absorption spectrum of the fiber [95].

Theoretical analyses represent a temperature sensor with a high sensitivity based on the MOF Sagnac interferometer [96]. Ethanol was inserted in the air holes of the MOF. Two big air holes were introduced for enhancing the birefringence and sensitivity of the proposed device. Simulation results showed that the proposed MOF temperature sensor achieved a high sensitivity of 14.7 nm/°C in the temperature range varies from 15 to 75 °C. In 2022, the silver mirror reaction was used for coating the silver film on the surface of the self-made MOF to stimulate the surface plasmon resonance effect, and polydimethylsiloxane (PDMS) with a high thermal-optical coefficient was coated on the silver film as temperature-sensitive material [97]. The MOF with silver and PDMS films was coupled with multimode fiber on both sides to form the temperature sensor. In this sensor system, the energy is coupled into the cladding of the microstructure fiber by a multimode fiber, and the surface plasmon resonance can be further excited in the MOF. The refractive index of PDMS changes with a change in the temperature of the external environment. The

proposed sensors exhibited a very high sensitivity of  $0.83 \text{ nm}/^\circ\text{C}$  and  $-0.84 \text{ nm}/^\circ\text{C}$  during heating and cooling for the temperature range of  $35\text{--}95 \text{ }^\circ\text{C}$ , respectively.

Apart from these sensing techniques, the researcher used nonlinear properties of the MOF for the sensing purpose. A unique fiber-optic soliton self-frequency shift (SSFS) temperature sensor was developed, which was built utilizing an in-house MOF [98]. SSFS-based sensing was systematically examined using this sensor with variations in average pump wavelength and pump power. The sensing performance of the proposed sensor was assessed experimentally and conceptually, subject to the average pump wavelength and pump power, by detecting the center wavelength shift of the 3 dB bandwidth of the soliton with temperature change. Greater sensitivity was achieved when the pump wavelength is longer while the average pump power was fixed. At an average pump power of 300 mW and a pump wavelength of 1600 nm, the maximum sensitivity of the proposed sensing device is  $1.759 \text{ nm}/^\circ\text{C}$ . A small fiber-optic temperature sensor is suggested and experimentally proven using refractive index liquid functionalized side-hole microstructured optical fibers (SHMOFs) [99]. The transmission spectrum of the suggested temperature sensor has been examined experimentally and theoretically. Multiple resonance dips in the transmission spectrum are present due to resonance coupling between the fundamental core mode and refractive index liquid rod modes, which may be adjusted by modifying ambient temperature. According to the experimental data, the maximum temperature sensitivity is  $13.1 \text{ nm}/^\circ\text{C}$  over a temperature range of  $80\text{--}100 \text{ }^\circ\text{C}$ .

Zhang et al. demonstrated a surface plasmon resonance (SPR) based temperature sensor made of a silver-coated multihole optical fiber [100]. The structure of the proposed sensor was comprised of an input lead-in MMF, a silver-coated multihole optical fiber, and an output lead-out MMF. The middle silver-coated multihole optical fiber (SMHOF) is filled with two types of thermo-sensitive liquid. In the previously reported sensors, the external temperature was monitored by measuring the wavelength shift of a single SPR peak. However, the proposed work utilizes the concept of dual SPR dips which ultimately improves the sensitivity and expanded the detection range. Here, in a single-optical-fiber structure, two distinguished SPR dips appeared at different wavelengths which are caused by adjusting the refractive index of two types of thermo-sensitive liquid moving in opposite directions with some temperature difference are excited. The illustrative view of the proposed SMHOF temperature sensor and the cross-section of a thermo-sensitive liquid-filled SMHOF are shown in Figure 8a,b, respectively. A linear relationship between the environmental temperature and the interval of the two SPR dips is demonstrated. The reported SMHOF temperature sensors offer a high sensitivity of  $7.72$  and  $-7.81 \text{ nm}/^\circ\text{C}$  in the range of  $20\text{--}60$  and  $-20\text{--}20 \text{ }^\circ\text{C}$ , respectively.

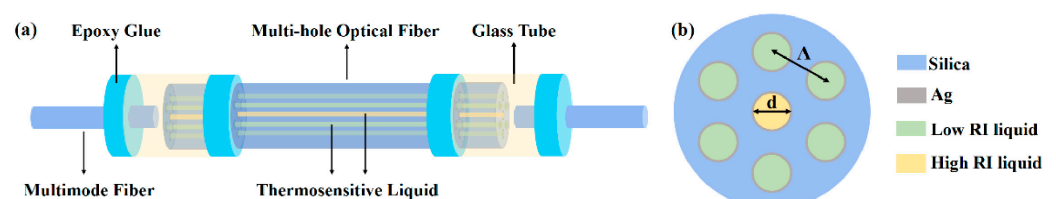


**Figure 8.** (a) Schematic diagram of the proposed SMHOF temperature sensor. (b) The cross-section of the SMHOF filled with thermo-sensitive liquids [reprinted with permission from [100] © The Optical Society].

**Advantages and Limitations:** The thermo-elastic deformation of MOF can be significantly smaller than that of normal fibers under the same heat impact, which is among its advantages. Additionally, the temperature equalization velocity in MOFs is higher than in conventional fibers. The thermal gradients in MOFs are lower than in conventional fibers. The size of the MOF, the number of air rods, how they are arranged, and other variables all affect how much these variations are worth. The fact that the air rods in MOFs may be filled with a variety of materials, such as a particular gas combination or

a certain kind of nanomaterial, is another crucial benefit of these fibers. This will make it possible to obtain fiber with special optical and thermal characteristics. For instance, compared to fiber-optic gyros based on ordinary optical fibers, employing MOFs with air rods loaded with thermally conductive nanoparticles, such as carbon nanotubes, can dramatically minimize temperature gradients (up to over 10 fold) in the optical fiber coil.

Table 1 summarized the different structures of the MOF with or without external material coating and selectively filled configuration used for temperature sensing.

**Table 1.** Summary of MOF-based temperature sensors.

Fiber Structure	Material	Temp. Range	Sensitivity	Refs.
D-shaped PCF	Benzene	10–70 °C	110 nm/°C	[16]
Metal-filled side-hole PCF	In Bi	18–86 °C 22.4–46 °C 21.6–70.7 °C	–7.38 nm/°C –9 nm/°C –1.80 nm/°C	[45]
PCF	Silver nanowire	10–40 °C	2.7 nm/°C	[47]
Alcohol-filled high birefringence PCF	Alcohol	8–34 °C	6.6 nm/°C	[49]
Capillary fiber with germanium-doped elliptical-shaped core	Indium	30–45 °C	8.40 ± 0.06 nm/°C	[50]
Nematic liquid crystal-filled PCF	Nematic liquid crystal (6CHBT)	44–53 °C	–3.90 nm/°C	[52]
PCF with a specially doped germanium core	Gold	0–500 °C	78 pm/°C	[61]
Dual-core PCF	N/A	30–900 °C	33.3 pm/°C	[65]
PCF	N/A	25–280 °C	–0.011 V/°C	[66]
Four-bridge double Y-shape core microstructure fiber	N/A	30–270 °C	12.5 pm/°C	[67]
Liquid-filled PCF	Gold	0–100 °C	3080 pm/°C	[74]
Liquid-filled PCF long period grating	Isopropanol	20–50 °C	1.356 nm/°C	[75]
MMF-PCF-MMF	PDMS on gold film	35–100 °C	–1.551 nm/°C	[82]
Hollow core fiber	PDMS	25–80 °C	–384 pm/°C	[83]

### 3. Conventional Silica Fibers

Single-mode fibers (SMFs), multimode fibers (MMFs), no-core fibers (NCF), multicore fibers (MCFs), etc., are the types of conventional fibers that are made of either fused silica and/or germanium-doped silica. These fibers are named based on their appearance; for example, an SMF contains a germanium core (8 µm) and fused silica cladding (125 µm), whereas the NCF contains only silica cladding of diameter of 125 µm. Optical fiber plays a crucial role in sensing elements to monitor several physical and chemical parameters such as chemical variations, strain, pressure, vibration, and temperature [101–104]. There are several ways of converting a temperature signal into an optical and then an electrical signal. The most popular used approach is to employ SMFs, MMFs, NCFs, MCFs, etc., as temperature sensors. Other than this, the application of the SMF–MMF–SMF structure was also exploited at a large scale [105–107]. The sensing mechanism of conventional fibers uses an amplified emission source to input broadband light into the sensor and the photodetector to detect the response. The measured temperature range relies on the used photodetector's sensitivity and the properties of the fiber which acts as a sensor. In this section, the current status of research on conventional fibers as temperature sensors is presented.

In 2012, Arun et al. reported the design and fabrication of SMF-based temperature sensor developed using the wet-etching method [108]. A dependency of sensitivity on etched fiber diameter was reported and explained. The sensor showed an insensitive functioning of an un-etched fiber and  $3.8 \mu\text{W}/^\circ\text{C}$  ( $0.2 \mu\text{W}/^\circ\text{C}$ ) while a high sensitivity for an  $11.2 \mu\text{m}$  ( $25 \mu\text{m}$ ) etched diameter. The sensor outcome was found to be appropriate for analog signal transmission over optical fiber through thermal modulation. For high-temperature monitoring, Tan et al. reported a partial-reflection-enabled compact FPI based sensor [55]. The FPI includes a SMF and a small core MOF. The FPI follows the basic principle of occurring partial Fresnel reflection at the interface of the two fibers and the end surface of the MOF. The compact and simple temperature sensor showed good sensing performance even at  $1000^\circ\text{C}$  and achieve an high sensitivity of  $17.7 \text{ pm}/^\circ\text{C}$  at  $1570 \text{ nm}$ . The sensor also finds its application in space-oriented high temperature-monitoring applications. In the same year, Yang et al. reported a liquid-sealed S-tapered fiber-based highly sensitive temperature sensor [109]. Here, the hermos-optic effect of liquid and thermal expansion of S-taper fiber makes the temperature sensor more sensitive. The length of the sensor varied from  $10$  to  $1 \text{ mm}$ . The fabricated sensor reported a high a sensitivity of  $-1.403 \text{ nm}/^\circ\text{C}$ . In 2013, Manoj et al. presented a comparative study of temperature sensors using the SMF–MMF–SMF structure using step and graded index MMFs [110]. Here,  $\text{GeO}_2$  with two different doping concentrations was employed in the core of the MMF. For the entire wavelength range of  $0.7$ – $1.6 \mu\text{m}$ , the temperature sensitivity of the proposed sensor with graded index MMFs was found larger ( $25$ – $285$  fold) than the step-index MMF.

Hao et al. reported a low-cost and simple temperature sensor using an SMF core-offset structure [111]. The schematic diagram of the sensor is shown in Figure 9. With the application of temperature over the core-offset structure, the output laser wavelength due to variation in pass-band varies.

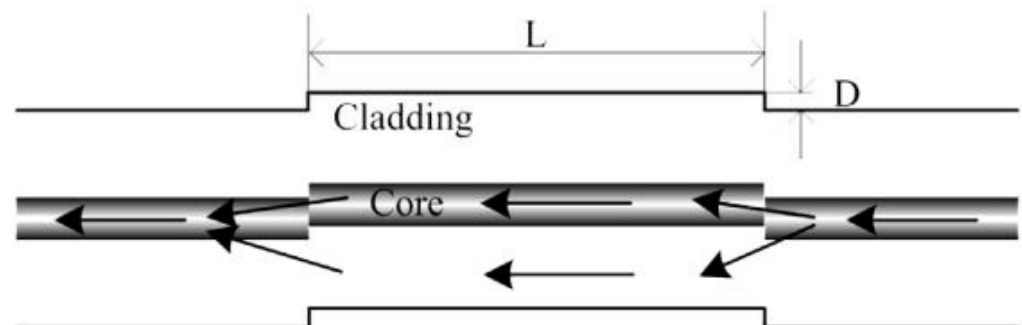


**Figure 9.** Schematic diagram of core-offset SMF based temperature sensor [111].

The experimental outcome showed the achievement of single-wavelength laser with the application of core-offset structure in the ring cavity. With the pump power of  $100 \text{ Mw}$ , the output laser peak power and SMSR of  $-8.93$  and  $47 \text{ dB}$ , respectively, has been found. For the temperature range of  $30$ – $270^\circ\text{C}$ , a temperature sensitivity of  $0.0449 \text{ nm}/^\circ\text{C}$  has been obtained. Compared to the previously reported sensors, the proposed sensor offered higher output power, higher SMSR, large measuring range, and lower cost and therefore can find its application in the laser sensing domain. Noor et al. proposed the use of the SMF–MMF–SMF structure following the multimode interference phenomenon as a temperature sensor [112]. The bent MMF unit, because of its small curvature radius, projects a balloon shape. The MMF was coated with acrylate coating which offers higher temperature sensitivity due to its higher thermos-optic coefficient. The work reported both simulated and experimental validation of the design and the results. For the temperature range of  $27$ – $31^\circ\text{C}$ , wavelength and intensity-based interrogation and temperature sensitivity of  $-25.1 \text{ nW}/^\circ\text{C}$  and  $-2060 \text{ pm}/^\circ\text{C}$  was obtained, respectively. In a similar work, Wildner et al. show the combination of two materials (glass particles and transparent oil/polymer) with different thermo-optic coefficient in the formation of

a temperature sensor [101]. Here, the key performance parameters that vary the sensing of temperature such as particle size, filling degree and length are varied. The work demonstrated the freedom to select materials in according with the desired output of the sensor. Small (large) differences in the thermo-optic coefficient of two materials are selected for a wide measuring range.

In 2017, Peng et al. reported a U-shaped bent single-mode fiber-based temperature sensor [113]. The U-shaped fiber has a double coating of outer nickel protection coating and inner. A linear relation between temperature and bend loss at a fixed wavelength and bending radius was reported. The inner coating worked as absorption coating and outer nickel coating worked as a protector of sensor. The proposed sensor offers temperature resolution and bends loss response of  $0.5\text{ }^{\circ}\text{C}$  and  $0.023\text{ dB}/^{\circ}\text{C}$ . Hence, the proposed sensor can also be used for monitoring temperature in harsh environments. Cai et al. proposed an optical fiber-based temperature sensor [114]. The sensor follows the modal interference phenomenon of modes that occur in a multimode fiber. The sensor includes the segment of a single-mode fiber, a hollow core fiber, and a no-core fiber with PDMS integrated over the cavity of a hollow core fiber. The high thermo-optic coefficient and the thermal-expansion coefficient of PDMS make the effective refractive index larger with the change in temperature and hence result in a good temperature sensor. Both the experimental and simulation results have been presented where the experimentally obtained results were found at par with the results obtained by simulation. A temperature sensitivity of  $580.6\text{ pm}/^{\circ}\text{C}$  in the range of  $28\text{--}50\text{ }^{\circ}\text{C}$  has been obtained. A similar work has been reported by Gao et al., where an optical fiber-based temperature sensor with a PDMS/silica hybrid structure based on the modal interference principle was demonstrated [83]. The hybrid structure was placed between two SMFs that act as the sensing unit. Here, PDMS was integrated to enhance the sensitivity by inserting it into the hollow core fiber to ultimately develop PDMS/silica hybrid fiber structure. The illustrative sensor structure is shown in Figure 10. Here, the PDMS-filled length, core diameter, and air-gap length were noted as 20 mm, 30  $\mu\text{m}$ , and 1 mm, respectively.

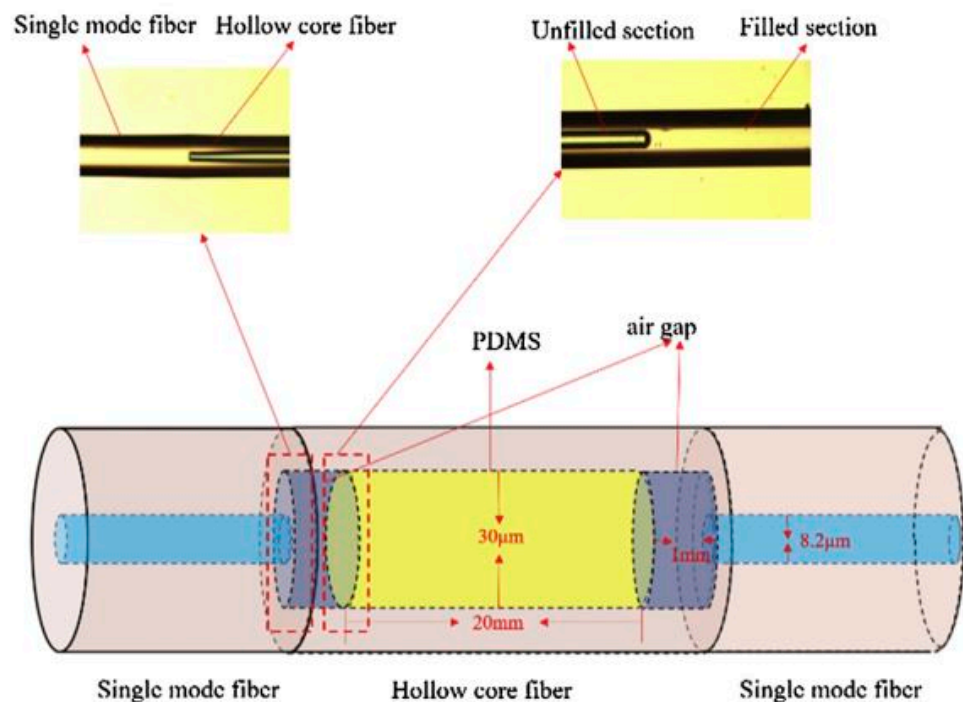
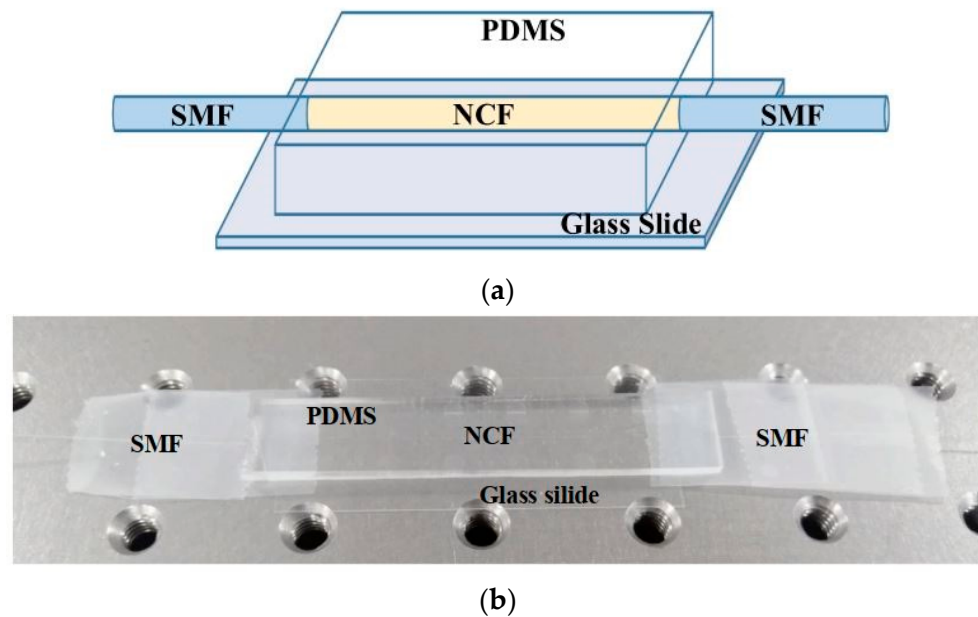


Figure 10. Temperature sensor with PDMS/silica hybrid fiber structure [83].

The hybrid fiber with different modes experiences the phase delay which is influenced by the external environmental conditions. Owing to the modal interference concept, the resonance wavelength shifted with respect to the variation in temperature. The experimental finding determined the sensor sensitivity to be  $-384 \text{ pm}/^\circ\text{C}$  for a temperature range of  $25\text{--}80 \text{ }^\circ\text{C}$ , with a hollow core fiber of core diameter of  $30 \text{ }\mu\text{m}$ . The proposed temperature sensor can be used to sense the real-time temperature in domains of Chemical, biological detection, and medical.

In 2019, Huang et al. proposed a temperature and refractive index sensor based on the MMF-SMF-MMF structure coated with a graphene-metal hybrid [115]. The sensitivity was improved by adding the graphene layer above or below of gold coating in the fiber. It was found that the refractive index sensitivity of the graphene-gold-Au on Ag nanoparticle film was higher than the conventional Au on Ag nanoparticle film, graphene-Au, or Au-graphene films. The sensitivity of graphene Au-Au@Ag NPs film ( $1591 \text{ nm}/\text{RIU}$ ) was higher than that of Au@Ag NPs ( $29 \text{ nm}/\text{RIU}$ ), graphene-Au ( $1224 \text{ nm}/\text{RIU}$ ), Au ( $1034 \text{ nm}/\text{RIU}$ ), and Au-graphene film ( $807 \text{ nm}/\text{RIU}$ )-modified MMF-SMF-MMF structures at a RI of 1.333. Similarly, polydimethylsiloxane (PDMS) was introduced to the graphene-Au on Ag nanoparticle film for sensing of temperature which exhibited a higher sensitivity of  $1.02 \text{ nm}/^\circ\text{C}$  with good repeatability. The proposed sensor finds its application in protection, environment, nano-medicine, and clean energy fields. Sun et al. presented a sensor with a single-mode fiber spliced with a multimode fiber on which a Bragg grating structure has been written [106]. The reported sensor with good reliability, repeatability, and accuracy finds its application in the sensing of high temperature and micro-bending. Temperature and micro-bending's measurement range was defined as  $0\text{--}900 \text{ }^\circ\text{C}$  and  $0\text{--}0.453 \text{ m}^{-1}$ . The temperature sensitivity and maximum bending sensitivity in the corresponding range were found to be  $13.4 \text{ pm}/^\circ\text{C}$  and  $23.03 \text{ dB}/\text{m}^{-1}$ . Similarly, the accuracy was measured of  $0.002\text{--}0.005 \text{ dB}$ . Similarly, in 2022, Xiaowei et al. reported a sensor with an arc-shaped misaligned structure MZI on an SMF [116]. A layer of composite material (UV-curable polymer) was coated over the sensor to improve the temperature sensitivity. Along with temperature sensitivity, the strain sensitivity was also monitored with negligible effect. The obtained result was validated from both theoretical and experiment analysis. Compared to previously reported sensors, the proposed temperature sensor showed an improved sensitivity of  $-0.953 \text{ nm}/^\circ\text{C}$ . Owing to simple manufacturing and small size, the proposed device may find its application in the domain of biology and chemistry.

Wang et al. presented a temperature sensor with an SMF-NCF-SMF structure with PDMS coating [18]. In this work, PDMS due to its negative thermos-optic coefficient and large thermal expansion coefficient (TEC) was employed to increase the TEC of no-core optical fiber to finally enhance the temperature sensitivity of the proposed sensor. The study reports the result obtained using both theoretical analysis (MATLAB) and experiment. The schematic and physical diagram of the sensor is shown in Figure 11.



**Figure 11.** (a) Structural and (b) physical pictures of the sensor chip [18].

The theoretical finding showed good agreement with the experimental results, with a temperature sensitivity of  $-260 \text{ pm}/^\circ\text{C}$ . In addition, the proposed sensor also offers strong resistance to external interference and mechanical damage, simple fabrication.

The multicore fiber (MCF)-based temperature sensor, due to its cost, easy of fabrication and thermal stability at high temperature, offers a beneficial alternative to a photonic crystal and fiber Bragg grating-based temperature sensor. Wales et al. proposed the experimental demonstration of MCF-based temperature sensors spliced between two SMF sections [117]. The device was calibrated both in gas and liquid mediums using a photodiode-based interrogator and shows a linear  $35 \text{ pm}/\text{shift}$  with respect to the change in temperature. The final sensor was packaged in  $0.559 \text{ mm}$  diameter stainless steel tube. In 2022, Josu et al. proposed a multicore fiber (MCF)-based temperature sensor which operates in a thermal range from  $-25$  to  $900^\circ\text{C}$ , where a K-type thermocouple was employed as a reference device [118]. The proposed sensor consists of a segment of a MCF spliced to a standard SMF. The proposed sensor is passive, easy to fabricate, compact and finds application in the industrial field that demands ultrahigh-sensitive temperature sensing.

**Advantages and Limitations:** In addition to these reviewed articles, some other articles utilized these conventional fibers to achieve superior sensing performance, as shown in Table 2. So far, the application of different kinds of fiber as standard fiber for temperature-sensing application has been presented. However, each variety has its own merits and demerits. The proposed fiber as a sensor offers the advantage of small size, low cost, higher output power, less detection limit, resistance to electromagnetic interference, remote detection and multiplexing. Moreover, a few of these fiber-based sensors suffer from the need for a larger measuring range and a narrower linewidth to measure the minute wavelength shift, fabrication complexity, and the employment of sophisticated equipment. Although plastic optical fibers comprise several advantages such as a large core diameter, a lower cost and are highly flexible, they fail to gain enough attention in temperature sensing because of some major drawbacks, i.e., lower bandwidth, high attenuation, shorter range, etc., compared to silica fibers.

**Table 2.** Summary of other conventional optical fiber-based temperature sensors.

Fiber Structure	Material	Temp. Range	Sensitivity	Refs.
SMF–MMF	N/A	0–900 °C	13.4 pm/°C	[106]
SMF–NCF–SMF	N/A	N/A	–260 pm/°C	[100]
arc-shaped misaligned MZI on SMF	N/A	N/A	–0.953 nm/°C	[116]
MMF–SMF–MMF	PDMS on graphene Au–Au@Ag NPs	N/A	1.02 nm/°C	[115]
SMF–HCF–SMF	PDMS	25–80 °C	–384 pm/°C	[83]
SMF–NCF–SMF	PDMS	28–50 °C	580.6 pm/°C	[114]
SMF–MMF–SMF	N/A	27–31 °C	–2060 pm/°C	[112]
core-offset SMF	N/A	30–270 °C	0.0449 nm/°C	[111]
S-tapered fiber	N/A	–	–1.403 nm/°C	[109]
FPI in SMF	N/A	1000 °C	17.7 pm/°C	[55]
SMF–SCPSF–SMF	N/A	200–1000 °C	106.64 pm/°C	[108]
multimode POF	N/A	25–110 °C	$1.04 \times 10^{-3} \text{ °C}^{-1}$	[119]

#### 4. Grating-Based Fibers

Nowadays, fiber Bragg grating (FBG) is considered as among the most popular optical components widely exploited in optical networking, physical and chemical sensing due to their ease of fabrication, small size, multiplexing feature, and low cost. An FBG comprises a periodic variation of the refractive index (RI) within the core of a single-mode fiber, which satisfies the phase matching condition between the fundamental mode and other modes, either the core mode or the cladding modes or radiation (or leaky) modes [120]. In 1978, Hill et al. fabricated and reported the first FBG in a germanium-doped core [121]. The grating was made by using the laser lithography technique to incorporate the permanent periodic variation of the refractive index in the fiber core.

The sensing principle of FBG-based fibers can be defined as the grating period, grating length, and the effective refractive index of such fibers that are affected by the variation in the surrounding media [122]. The change in the outer environment leads to the change in its resonance condition; consequently, the variation in resonance wavelength takes place. Based on the property of these gratings, it can be classified into three categories: (1) fiber Bragg grating (FBG), (2) long-period fiber grating (LPFG), and (3) tilted FBG (TFBG). The grating-based optical fibers gain huge attention in physical and chemical sensing due to their unique features of immunity to electromagnetic interferences, compact size, highly sensitive, multiplexing capability, and in situ monitoring. Owing to their design of label-free monitoring of the surrounding environment, grating-based sensors, such as FBG, LPG, etched FBG, and TFBG, have attracted extensive attention in order to develop physical and chemical sensors. In grating-based fibers, the Bragg wavelength is calculated by the refractive index modulation period ( $L$ ) and the effective refractive index of the fiber ( $n_{eff}$ ), and shown by the following relation [123]:

$$\lambda_{Bragg} = 2n_{eff}L \quad (1)$$

A change in the refractive index of the fiber is observed, under the variation of the temperature, leading to a linear drift in the value of the Bragg wavelength. Temperature monitoring using grating fibers can be easily achieved by demodulating the Bragg wavelength variation. Compared to other optical fiber sensors, the grating-based temperature sensors showed several advantages including good linearity, high stability, multiplexing capability, and mass production, which have been used widely in commercialization.

In 2014, Zaynetdinov et al. developed an FBG-based temperature sensor with an operating range of 2–400 K along with a temperature resolution better than 10 mK for temperatures below 12 K [124]. The sensing head was fabricated from a polyimide-coated optical fiber. The response was achieved by mounting the section of the fiber on a polytetrafluoroethylene tape, which has a non-negligible coefficient of thermal expansion down to <4 K. The sensors exhibited excellent stability over multiple trials along with the superior repeatability of temperature cycles. In 2016, Hsiao et al. reported a chromium nitride (CrN)-coated FBG sensor for extreme temperature environments [125]. The sensing configuration was fabricated by depositing CrN using the physical vapor deposition (PVD) technique. During the sputtering process, the pressure of the deposition system was fixed at  $6 \times 10^{-3}$  Torr, with 70 W power applied to the Cr target. The film was deposited for 15 min to achieve an approximate thickness of 2  $\mu\text{m}$  over the FBG. The sensor was based on a wavelength interrogation technique analyzed by utilizing an optical spectrum analyzer (OSA). The reflection spectra of the fabricated sensor were monitored and compared with bare FBG for temperatures varying from 100 to 650  $^{\circ}\text{C}$ . The results exhibited that the CrN-coated FBG sensor gives a 14.0  $\text{pm}/^{\circ}\text{C}$  greater temperature sensitivity compared to the bare FBG fiber without CrN.

In 2018, Dong et al. reported the utilization of graphene oxide (GO) as a sensing layer integrated over FBG for simultaneous pressure and temperature monitoring [126]. The sensing configuration was based on the Fabry–Perot interferometer (FPI). The light reflectors of the fabricated FPI sensor comprise a thin graphene film coated over the end facet of FBG, as shown in Figure 12. The sensor exhibited good sensitivities of 501.4  $\text{nm}/\text{kPa}$  and 306.2  $\text{nm}/^{\circ}\text{C}$ , for pressure and temperature, respectively. The introduction of FBG along with GO can successfully prevent the cross-impact of the FPI sensor. Following the improvement of sensing performance, in the same year of 2018, Jasmi et al. also reported an FBG-based temperature sensor by utilizing polyurethane–GO nanocomposite as a sensing layer [127]. The physical, chemical, and conductivity of PU–GO were observed to be improved after introducing GO in the pristine PU. The thermogravimetric analysis exhibited that the thermal stability of PU improved to 217  $^{\circ}\text{C}$  because of the strong intermolecular interaction with graphene flakes leading to an enhanced in sensing performance. The sensing material was coated over FBG using dip-coating to obtain uniform thickness, while the sensing performance of the device was evaluated for a wide range of temperatures varying from 25 to 60  $^{\circ}\text{C}$ . The sensor exhibited good linearity along with an improved sensitivity of 6  $\text{pm}/^{\circ}\text{C}$ .

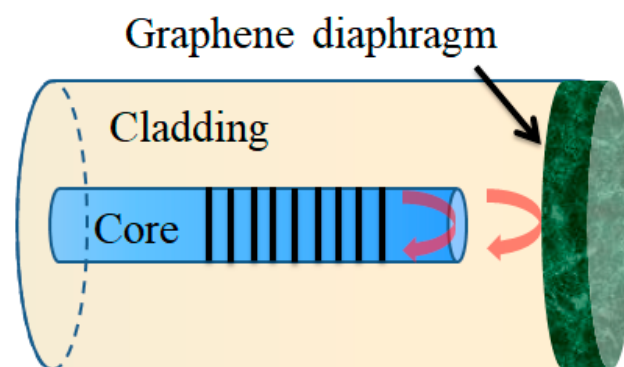


**Figure 12.** FBG sensor integrated with graphene for simultaneous detection of temperature and pressure.

In 2019, Cheng et al. introduced strontium titanate ( $\text{SrTiO}_3$ ) thin film coated over FBG using pulsed laser deposition for temperature sensing [128].  $\text{SrTiO}_3$  is a ferroelectric thin film with typical perovskite-like structures with remarkable optical, dielectric, and photoelectric properties. For deposition, the FBG was immersed in the acetone solution for 5 min to remove the buffer coating, which was later coated with 271.5 nm thick  $\text{SrTiO}_3$

film on the cladding. In order to study the thermal sensing performance of the FBG, a concatenated optical path, two optical paths based on a Michelson interferometer (MI) and one based on Sagnac interferometer, were fabricated using SrTiO<sub>3</sub>-coated FBG and another bare FBG. The sensing performance of the device was investigated for a wide range of temperatures varying from 40 to 150 °C. The sensitivity for each sensing configuration was observed to be 9.0 pm/°C, 10.5 pm/°C, and 11.4 pm/°C, for two MI and one Sagnac interferometer, respectively. Later in 2020, Gao et al. reported a dual-parameter fiber sensor to consist of a few-mode fiber and FBG for simultaneous detection of strain and temperature variation [129]. The sensing configuration was fabricated using a 6.5 cm length of few-mode fiber offset spliced with a single-mode fiber (SMF), as shown in Figure 13. The temperature and strain were measured simultaneously due to the different sensitivities of the obtained spectrum dips. The fabricated sensor exhibited a good temperature sensitivity of −34.3 and 10.7 pm/°C, and strain sensitivities of −2 pm/μ $\epsilon$  and 0.67 pm/μ $\epsilon$ , respectively. The fabricated device showed good potential in fields of dual-parameter measurement due to its simple configuration, cost-effectiveness, and compact structure.

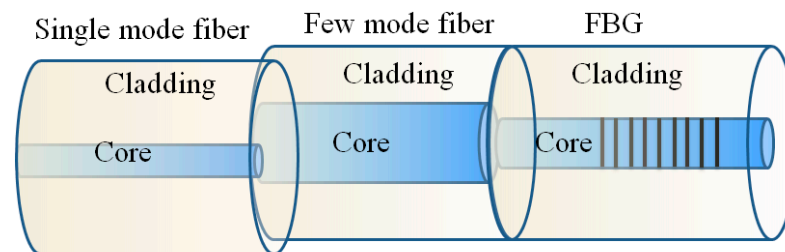


**Figure 13.** Sensing configuration for strain and temperature monitoring.

Later in 2021, Chen et al. reported an optical fiber sensor based on a fiber surface waveguide and Bragg grating for simultaneous monitoring of refractive index and temperature variations [130]. The device consists of two FBGs fabricated by a femtosecond laser, one of which is situated in the fiber core for temperature sensing; the other is located in the fiber surface waveguide for both temperature and RI measurements. The fabricated device exhibited good RI and temperature sensitivities of 10.3 nm/RIU and 9.94 pm/°C, respectively. Later in 2022, Esposito et al. reported a miniaturized metallic package for FBG sensors to improve the temperature sensitivity and eliminate the cross-sensitivities to mechanical effects of impulsive forces or strain [131]. The packaging of the device required the encapsulation of FBG into a steel tube, which was later placed inside another larger steel tube, where the fiber was kept loose to prevent any mechanical effect from transferring to the grating. The fabricated device exhibited a linear temperature response in the range varying from 5 to 50 °C along with a high sensitivity of 28.9 pm/°C, which was nearly 3-fold higher than the standard FBG. In addition to sensing performance, the device also shows a rapid response time of 5 s when tested under temperature of 20 °C. In addition of these reported FBG-based sensors, some other sensor also listed in Table 3, which shows an excellent performance and competitive response.

**Table 3.** Summary of FBG-based temperature sensors.

Fiber Structure	Material	Temp. Range	Sensitivity	Ref.
FBG	N/A	5–50 °C	28.9 pm/°C	[131]
FBG	N/A	27–427 °C	14.42 pm/°C	[132]
FBG	N/A	–5–35 °C	35 mV/°C	[133]
Sapphire-FBG	N/A	0–1800 °C	41.2 pm/°C	[134]
Sapphire-FBG	N/A	0–1200 °C	30.19 pm/°C	[135]
FBG	N/A	0–1000 °C	18.2 pm/°C	[136]
FBG	N/A	40–260 °C	13 pm/°C	[137]
FBG	titanium nitride	25 to –195 °C	10.713 pm/°C	[138]
Tapered FBG	gold	0–50 °C	9.893 pm/°C	[139]
Hollow core Bragg fiber	N/A	600 °C	25.925 pm/°C	[140]
FBG	poly (methyl methacrylate)	15–35 °C	–0.080 nm/°C	[141]
FBG	polydimethylsiloxane	20, 30, 40 and 50 °C	4.88, 5.15, 4.53 and 4.38 nm/°C	[142]
FBG	Polymer	80 °C	9.33 nm/°C	[143]

**Advantages and Limitations:** The grating-based optical fiber gains huge development in temperature sensing due to its salient features such as high sensitivity, a fast response time, excellent stability over a larger time, and ease of multiplexing, enabling simultaneous temperature monitoring at multiple points along the length of the fiber. In addition to these advantages, the grating-based fiber suffers several limitations such as limited temperature range, highly expensive, signal processing complexity, strain sensitivity, and polarization sensitivity. These limitations may cause false or mixed output results, and differentiating the output data are a difficult task itself.

### 5. Future Prospects and Challenges

With the advancement of micro- and nano-technology and the development of fibers with unique optical characteristics, there is little question that designs and fabrications of innovative microstructured fiber-optic sensors will continue to be a thriving research topic. Opportunities and challenges coexist simultaneously in the work to be performed on microstructured fiber-optic sensors in the future. These include the ability to measure multiple parameters simultaneously and with selectivity. Although several microstructured fiber-optic sensors with dual-parameter measuring capabilities have been proposed to date, efforts should be made to reduce measurement error and expand dual-parameter measurement to three-parameter or even more parameter characterizations because the cross-talk effect is typically brought on by more than two parameters in many applications. Even greater sensitivity also requires MOF sensors with exceptionally high accuracies for more exact measurements. Sensing in severe conditions is required including those in high pressure, strong radiation, and extremely low or high temperatures. An intelligent MOF sensor should have functionalities that can be changed and adjusted in response to various target samples and circumstances. A more adaptable and potent sensor architecture is desirable. The robustness of the microscopic structures is the key to the sensing performance and longevity of the device; therefore, better packaging without sacrificing sensitivity will be the future goal. Additionally, there is a need for a simplified and easy fabrication process for the MOF sensor. One main aspect of the MOF-based sensor is to control the attenuation loss which is more important for the practical application.

Real-time monitoring of temperature in patients in the inpatient floor and ICU with small devices that can monitor the fluctuations in real time as with telemetry can be extremely useful in patients with pneumonia and or sepsis and any other infections especially those who are intubated and unable to speak in critical care units. This will

enable more efficient detection of hospital-acquired infections and will be helpful for quicker reaction to tackle possible infection in patients. In a normal clinical setting, the patient has to inform the nurse that they have a fever or the nurse has to keep checking the temperature of the patient at regular intervals. With a real-time temperature-monitoring device, it would be easier and faster to detect a new infection and nip it in the bud before it goes on to form a major infection or abscess and may be useful in ultimately reducing a lot of incidences of sepsis.

Temperature monitoring is often overlooked in critical care when compared to other factors such as pulse oximetry and telemetry but it is an important factor, a biological alarm that signals infection or some other abnormality in the patient. So this technology can be extremely useful in not only detecting cases of COVID-19 or flu during pandemics for screening a large number of people easily but it can also providing a means to monitor critically ill patients and give the doctors a head start in treating the infection before it becomes worse. This can revolutionize not just screening but also patient monitoring.

Each fiber comprises unique advantages and certain limitations. Multimode fibers contain a large core diameter, enabling a larger number of modes of propagation. The special feature makes such fibers more sensitive to the variation of temperature compared to the SMF. Additionally, such fibers are also robust in nature and suffer a lower bending loss, making them ideal for any harsh environments. These unique features make them the most suitable candidate for distributed temperature-sensing systems, e.g., Raman and Brillouin scattering-based temperature sensors, whereas multicore fibers contain multiple cores, which are generally used for temperature monitoring in a distributed manner. The temperature-induced changes in the refractive index value of the core cause variation in the transmission of light, which can be monitored to determine the temperature. The advantage of multicore fibers is that they can measure temperature at multiple points simultaneously over long distances, which makes them an ideal candidate for structural health monitoring applications. PCFs are specialized fibers with a unique structure that enables the propagation of light in a photonic bandgap, therefore making them highly sensitive to temperature variation. The bandgap shifts with temperature variation and can be measured to determine the temperature. These fibers also have a very low bending loss and excellent temperature stability, which makes them a superior candidate for high-temperature monitoring. PCFs are suitable for temperature sensing in high-temperature environments, e.g., furnaces, power plants, and engines. In summary, the MMF, multicore fibers, and PCFs offer unique advantages for temperature-monitoring applications along with the feature of distributed temperature sensing, high-temperature stability, and large temperature range.

## 6. Conclusions

In this review article, the role of various types of optical fibers and their sensing approach along with the sensor design, sensing material, working principle, and sensing performance including selectivity, sensitivity, and linearity are discussed and presented in detail. This paper provides a comprehensive review of the development of optical fiber-based temperature sensors in recent decades. Each sensing configuration comprises different structures and sensing material to achieve high sensitivity, which is listed and discussed for each sensor. New ideas and approaches to improve the sensing performance of such devices are also suggested in the future prospects section. Today, the increasing growth in the fields of optics, electronics, materials science, and data analysis has opened up a new path for study which can be expanded to include these principles for high precision and accuracy.

**Author Contributions:** Conceptualization, A.K.P. and S.K.; methodology, R.K.G., A.K.P. and S.K.; validation, A.K.P. and S.K.; formal analysis, R.K.G., A.K.P., S.K., S.D.G. and M.C.M.; writing—original draft preparation, R.K.G., S.K., A.K.P., S.D.G. and M.C.M.; writing—review and editing, R.K.G., A.K.P.

and S.K.; supervision, R.K.G. and S.K.; funding and project administration, A.K.P. All authors have read and agreed to the published version of the manuscript.

**Funding:** This research received no external funding.

**Institutional Review Board Statement:** Not applicable.

**Informed Consent Statement:** Not applicable.

**Data Availability Statement:** Not applicable.

**Conflicts of Interest:** The authors declare no conflict of interest.

## References

1. Ma, S.; Xu, Y.; Pang, Y.; Zhao, X.; Li, Y.; Qin, Z.; Liu, Z.; Lu, P.; Bao, X. Optical Fiber Sensors for High-Temperature Monitoring: A Review. *Sensors* **2022**, *22*, 5722. [[CrossRef](#)] [[PubMed](#)]
2. Childs, P.R.N.; Greenwood, J.R.; Long, C.A. Review of temperature measurement. *Rev. Sci. Instrum.* **2000**, *71*, 2959–2978. [[CrossRef](#)]
3. Yang, S.; Homa, D.; Heyl, H.; Theis, L.; Beach, J.; Dudding, B.; Acord, G.; Taylor, D.; Pickrell, G.; Wang, A. Application of Sapphire-Fiber-Bragg-Grating-Based Multi-Point Temperature Sensor in Boilers at a Commercial Power Plant. *Sensors* **2019**, *19*, 3211. [[CrossRef](#)]
4. Willsch, M.; Bosselmann, T.; Flohr, P.; Kull, R.; Ecke, W.; Latka, I.; Fischer, D.; Thiel, T. Design of Fiber Optical High Temperature Sensors for Gas Turbine Monitoring. In Proceedings of the 20th International Conference on Optical Fibre Sensors, Edinburgh, UK, 5 October 2009; Volume 7503, p. 75037R. [[CrossRef](#)]
5. Atkins, R.A.; Gardner, J.H.; Gibler, W.N.; Lee, C.E.; Oakland, M.D.; Spears, M.O.; Swenson, V.P.; Taylor, H.F.; McCoy, J.J.; Beshouri, G. Fiber-optic pressure sensors for internal combustion engines. *Appl. Opt.* **1994**, *33*, 1315. [[CrossRef](#)] [[PubMed](#)]
6. Watson, J.; Castro, G. A review of high-temperature electronics technology and applications. *J. Mater. Sci. Mater. Electron.* **2015**, *26*, 9226–9235. [[CrossRef](#)]
7. Gao, S.; Wang, L.; Feng, C. Multi-Spectral Pyrometer for Gas Turbine Blade Temperature Measurement. In Proceedings of the SPIE Optical Engineering + Applications, San Diego, CA, USA, 17–21 August 2014; Kazemi, A.A., Kress, B.C., Mendoza, E.A., Eds.; 2014; p. 920217.
8. Zhang, L.; Zhu, Y.; Jiang, M.; Wu, Y.; Deng, K.; Ni, Q. Body Temperature Monitoring for Regular COVID-19 Prevention Based on Human Daily Activity Recognition. *Sensors* **2021**, *21*, 7540. [[CrossRef](#)] [[PubMed](#)]
9. Costanzo, S.; Flores, A. A Non-Contact Integrated Body-Ambient Temperature Sensors Platform to Contrast COVID-19. *Electronics* **2020**, *9*, 1658. [[CrossRef](#)]
10. Bielska, S.; Sibinski, M.; Lukasik, A. Polymer temperature sensor for textronic applications. *Mater. Sci. Eng. B* **2009**, *165*, 50–52. [[CrossRef](#)]
11. Wawrzynczyk, D.; Bednarkiewicz, A.; Nyk, M.; Strek, W.; Samoc, M. Neodymium(iii) doped fluoride nanoparticles as non-contact optical temperature sensors. *Nanoscale* **2012**, *4*, 6959. [[CrossRef](#)]
12. Kus, A.; Isik, Y.; Cakir, M.; Coşkun, S.; Özdemir, K. Thermocouple and Infrared Sensor-Based Measurement of Temperature Distribution in Metal Cutting. *Sensors* **2015**, *15*, 1274–1291. [[CrossRef](#)]
13. Jun, S.; Kochan, O. Investigations of Thermocouple Drift Irregularity Impact on Error of their Inhomogeneity Correction. *Meas. Sci. Rev.* **2014**, *14*, 29–34. [[CrossRef](#)]
14. Nie, B.; He, X.; Zhang, C.; Li, X.; Li, H. Temperature measurement of gas explosion flame based on the radiation thermometry. *Int. J. Therm. Sci.* **2014**, *78*, 132–144. [[CrossRef](#)]
15. Pathak, A.K.; Viphavakit, C. A review on all-optical fiber-based VOC sensors: Heading towards the development of promising technology. *Sens. Actuators A Phys.* **2022**, *338*, 113455. [[CrossRef](#)]
16. Mollah, M.A.; Islam, S.M.R.; Yousufali, M.; Abdulrazak, L.F.; Hossain, M.B.; Amiri, I.S. Plasmonic temperature sensor using D-shaped photonic crystal fiber. *Results Phys.* **2020**, *16*, 102966. [[CrossRef](#)]
17. Cheng, T.; Li, X.; Li, S.; Yan, X.; Zhang, X.; Wang, F. Surface plasmon resonance temperature sensor based on a photonic crystal fiber filled with silver nanowires. *Appl. Opt.* **2020**, *59*, 5108. [[CrossRef](#)] [[PubMed](#)]
18. Wang, Z.; Chen, D.; Yang, X.; Liang, S.; Sun, X. Temperature sensor of single-mode-no-core-single-mode fiber structure coated with PDMS. *Opt. Fiber Technol.* **2022**, *68*, 102793. [[CrossRef](#)]
19. Savovic, S.; Kovacevic, M.S.; Bajic, J.S.; Stupar, D.Z.; Djordjevich, A.; Zivanov, M.; Drljaca, B.; Simovic, A.; Oh, K. Temperature Dependence of Mode Coupling in low-NA Plastic Optical Fibers. *J. Light. Technol.* **2015**, *33*, 89–94. [[CrossRef](#)]
20. Kreger, S.T.; Sang, A.K.; Gifford, D.K.; Froggatt, M.E. Distributed strain and temperature sensing in plastic optical fiber using Rayleigh scatter. In Proceedings of the Fiber Optic Sensors and Applications VI, Orlando, FL, USA, 27 April 2009; Udd, E., Du, H.H., Wang, A., Eds.; 2009; Volume 7316, p. 73160A.
21. Chu, C.-S.; Lo, Y.-L. A Plastic Optical Fiber Sensor for the Dual Sensing of Temperature and Oxygen. *IEEE Photonics Technol. Lett.* **2008**, *20*, 63–65. [[CrossRef](#)]

22. Liao, C.R.; Wang, D.N. Review of femtosecond laser fabricated fiber Bragg gratings for high temperature sensing. *Photonic Sens.* **2013**, *3*, 97–101. [[CrossRef](#)]
23. Markos, C.; Travers, J.C.; Abdolvand, A.; Eggleton, B.J.; Bang, O. Hybrid photonic-crystal fiber. *Rev. Mod. Phys.* **2017**, *89*, 045003. [[CrossRef](#)]
24. Chaudhary, S.; Amphawan, A. Solid core PCF-based mode selector for MDM-Ro-FSO transmission systems. *Photonic Netw. Commun.* **2018**, *36*, 263–271. [[CrossRef](#)]
25. Amphawan, A.; Chaudhary, S.; Neo, T.-K.; Kakavand, M.; Dabbagh, M. Radio-over-free space optical space division multiplexing system using 3-core photonic crystal fiber mode group multiplexers. *Wirel. Netw.* **2021**, *27*, 211–225. [[CrossRef](#)]
26. Pathak, A.K.; Ghosh, S.; Gangwar, R.K.; Rahman, B.M.A.; Singh, V.K. Metal Nanowire Assisted Hollow Core Fiber Sensor for an Efficient Detection of Small Refractive Index Change of Measurand Liquid. *Plasmonics* **2019**, *14*. [[CrossRef](#)]
27. Pathak, A.K.; Rahman, B.M.A.; Viphavakit, C. Nanowire Embedded Micro-Drilled Dual-Channel Approach to Develop Highly Sensitive Biosensor. *IEEE Photonics Technol. Lett.* **2022**, *34*, 707–710. [[CrossRef](#)]
28. Kumar Vyas, A.; Kumar Gangwar, R.; Kumar, S. Elliptical air hole PCF-based low-cost sensor for refractive index and temperature detection: Design and analysis. *Opt. Fiber Technol.* **2022**, *73*, 103060. [[CrossRef](#)]
29. Gangwar, R.K.; Pathak, A.K.; Qin, J.; Wang, X. Physics of photonic crystals and applications. In *Modern Luminescence from Fundamental Concepts to Materials and Applications*; Elsevier: Amsterdam, The Netherlands, 2023; pp. 313–327.
30. Gangwar, R.K.; Singh, V.K. Highly Sensitive Surface Plasmon Resonance Based D-Shaped Photonic Crystal Fiber Refractive Index Sensor. *Plasmonics* **2017**, *12*, 1367–1372. [[CrossRef](#)]
31. De, M.; Gangopadhyay, T.K.; Singh, V.K. Prospects of Photonic Crystal Fiber as Physical Sensor: An Overview. *Sensors* **2019**, *19*, 464. [[CrossRef](#)]
32. Russell, P. Photonic Crystal Fibers. *Science* **2003**, *299*, 358–362. [[CrossRef](#)]
33. Knight, J.C. Photonic crystal fibres. *Nature* **2003**, *424*, 847–851. [[CrossRef](#)]
34. Larsen, T.; Bjarklev, A.; Hermann, D.; Broeng, J. Optical devices based on liquid crystal photonic bandgap fibres. *Opt. Express* **2003**, *11*, 2589. [[CrossRef](#)]
35. Du, F.; Lu, Y.-Q.; Wu, S.-T. Electrically tunable liquid-crystal photonic crystal fiber. *Appl. Phys. Lett.* **2004**, *85*, 2181–2183. [[CrossRef](#)]
36. Haakestad, M.W.; Alkeskjold, T.T.; Nielsen, M.D.; Scolari, L.; Riishede, J.; Engan, H.E.; Bjarklev, A. Electrically tunable photonic bandgap guidance in a liquid-crystal-filled photonic crystal fiber. *IEEE Photonics Technol. Lett.* **2005**, *17*, 819–821. [[CrossRef](#)]
37. Alkeskjold, T.T.; Lægsgaard, J.; Bjarklev, A.; Hermann, D.S.; Anawati, A.; Broeng, J.; Li, J.; Wu, S.-T. All-optical modulation in dye-doped nematic liquid crystal photonic bandgap fibers. *Opt. Express* **2004**, *12*, 5857. [[CrossRef](#)] [[PubMed](#)]
38. Steinvurzel, P.; Eggleton, B.J.; de Sterke, C.M.; Steel, M.J. Continuously tunable bandpass filtering using high-index inclusion microstructured optical fibre. *Electron. Lett.* **2005**, *41*, 463. [[CrossRef](#)]
39. Alkeskjold, T.T.; Bjarklev, A. Electrically controlled broadband liquid crystal photonic bandgap fiber polarimeter. *Opt. Lett.* **2007**, *32*, 1707. [[CrossRef](#)] [[PubMed](#)]
40. Qian, W.; Zhao, C.-L.; Wang, Y.; Chan, C.C.; Liu, S.; Jin, W. Partially liquid-filled hollow-core photonic crystal fiber polarizer. *Opt. Lett.* **2011**, *36*, 3296. [[CrossRef](#)]
41. Jha, R.; Villatoro, J.; Badenes, G.; Pruneri, V. Refractometry based on a photonic crystal fiber interferometer. *Opt. Lett.* **2009**, *34*, 617. [[CrossRef](#)] [[PubMed](#)]
42. Li, B.; Sheng, Z.; Wu, M.; Liu, X.; Zhou, G.; Liu, J.; Hou, Z.; Xia, C. Sensitive real-time monitoring of refractive indices and components using a microstructure optical fiber microfluidic sensor. *Opt. Lett.* **2018**, *43*, 5070. [[CrossRef](#)]
43. Canales, A.; Jia, X.; Froriep, U.P.; Koppes, R.A.; Tringides, C.M.; Selvidge, J.; Lu, C.; Hou, C.; Wei, L.; Fink, Y.; et al. Multifunctional fibers for simultaneous optical, electrical and chemical interrogation of neural circuits in vivo. *Nat. Biotechnol.* **2015**, *33*, 277–284. [[CrossRef](#)]
44. Li, X.; Lin, S.; Liang, J.; Zhang, Y.; Oigawa, H.; Ueda, T. Fiber-Optic Temperature Sensor Based on Difference of Thermal Expansion Coefficient Between Fused Silica and Metallic Materials. *IEEE Photonics J.* **2012**, *4*, 155–162. [[CrossRef](#)]
45. Reyes-Vera, E.; Cordeiro, C.M.B.; Torres, P. Highly sensitive temperature sensor using a Sagnac loop interferometer based on a side-hole photonic crystal fiber filled with metal. *Appl. Opt.* **2017**, *56*, 156. [[CrossRef](#)] [[PubMed](#)]
46. Yang, H.; Wang, S.; Wang, X.; Wang, J.; Liao, Y. Temperature Sensing in Seawater Based on Microfiber Knot Resonator. *Sensors* **2014**, *14*, 18515–18525. [[CrossRef](#)] [[PubMed](#)]
47. Lu, Y.; Wang, M.T.; Hao, C.J.; Zhao, Z.Q.; Yao, J.Q. Temperature Sensing Using Photonic Crystal Fiber Filled With Silver Nanowires and Liquid. *IEEE Photonics J.* **2014**, *6*, 1–7. [[CrossRef](#)]
48. Reyes-Vera, E.; Gómez-Cardona, N.D.; Chesini, G.; Cordeiro, C.M.B.; Torres, P. Temperature sensibility of the birefringence properties in side-hole photonic crystal fiber filled with Indium. *Appl. Phys. Lett.* **2014**, *105*, 201101. [[CrossRef](#)]
49. Qian, W.; Zhao, C.-L.; He, S.; Dong, X.; Zhang, S.; Zhang, Z.; Jin, S.; Guo, J.; Wei, H. High-sensitivity temperature sensor based on an alcohol-filled photonic crystal fiber loop mirror. *Opt. Lett.* **2011**, *36*, 1548. [[CrossRef](#)]
50. Chesini, G.; Osorio, J.H.; Serrao, V.A.; Franco, M.A.R.; Cordeiro, C.M.B. Metal-Filled Embedded-Core Capillary Fibers as Highly Sensitive Temperature Sensors. *IEEE Sensors Lett.* **2018**, *2*, 1–4. [[CrossRef](#)]
51. Xie, J.; Xu, B.; Li, Y.; Kang, J.; Shen, C.; Wang, J.; Jin, Y.; Liu, H.; Ni, K.; Dong, X.; et al. High-sensitivity temperature sensor based on a droplet-like fiber circle. *Appl. Opt.* **2014**, *53*, 4085. [[CrossRef](#)]

52. Hu, D.J.J.; Long Lim, J.; Cui, Y.; Milenko, K.; Wang, Y.; Shum, P.P.; Wolinski, T. Fabrication and Characterization of a Highly Temperature Sensitive Device Based on Nematic Liquid Crystal-Filled Photonic Crystal Fiber. *IEEE Photonics J.* **2012**, *4*, 1248–1255. [[CrossRef](#)]
53. Chen, T.; Wang, Q.; Chen, R.; Zhang, B.; Jewart, C.; Chen, K.P.; Maklad, M.; Swinehart, P.R. Distributed high-temperature pressure sensing using air-hole microstructural fibers. *Opt. Lett.* **2012**, *37*, 1064. [[CrossRef](#)]
54. Li, X.; Sun, Q.; Liu, D.; Liang, R.; Zhang, J.; Wo, J.; Shum, P.P.; Liu, D. Simultaneous wavelength and frequency encoded microstructure based quasi-distributed temperature sensor. *Opt. Express* **2012**, *20*, 12076. [[CrossRef](#)]
55. Tan, X.; Geng, Y.; Li, X.; Gao, R.; Yin, Z. High temperature microstructured fiber sensor based on a partial-reflection-enabled intrinsic Fabry–Perot interferometer. *Appl. Opt.* **2013**, *52*, 8195. [[CrossRef](#)] [[PubMed](#)]
56. Poulton, C.G.; Schmidt, M.A.; Pearce, G.J.; Kakarantzas, G.; Russell, P.S.J. Numerical study of guided modes in arrays of metallic nanowires. *Opt. Lett.* **2007**, *32*, 1647. [[CrossRef](#)] [[PubMed](#)]
57. Hou, J.; Bird, D.; George, A.; Maier, S.; Kuhlmeier, B.; Knight, J.C. Metallic mode confinement in microstructured fibres. *Opt. Express* **2008**, *16*, 5983. [[CrossRef](#)] [[PubMed](#)]
58. Schmidt, M.A.; Prill Sempere, L.N.; Tyagi, H.K.; Poulton, C.G.; Russell, P.S.J. Waveguiding and plasmon resonances in two-dimensional photonic lattices of gold and silver nanowires. *Phys. Rev. B* **2008**, *77*, 033417. [[CrossRef](#)]
59. Sazio, P.J.A. Microstructured Optical Fibers as High-Pressure Microfluidic Reactors. *Science* **2006**, *311*, 1583–1586. [[CrossRef](#)] [[PubMed](#)]
60. Harrington, J.A. A Review of IR Transmitting, Hollow Waveguides. *Fiber Integr. Opt.* **2000**, *19*, 211–227. [[CrossRef](#)]
61. Favero, F.C.; Becker, M.; Spittel, R.; Rothhardt, M.; Kobelke, J.; Bartelt, H. Micro-structured fiber interferometer as sensitive temperature sensor. *Photonic Sens.* **2013**, *3*, 208–213. [[CrossRef](#)]
62. Luan, N.; Wang, R.; Lv, W.; Lu, Y.; Yao, J. Surface Plasmon Resonance Temperature Sensor Based on Photonic Crystal Fibers Randomly Filled with Silver Nanowires. *Sensors* **2014**, *14*, 16035–16045. [[CrossRef](#)]
63. Luan, N.-N.; Wang, R.; Lu, Y.; Yao, J.-Q. Simulation of surface plasmon resonance temperature sensor based on liquid mixture-filling microstructured optical fiber. *Opt. Eng.* **2014**, *53*, 067103. [[CrossRef](#)]
64. Geng, Y.; Li, X.; Tan, X.; Deng, Y.; Hong, X. Compact and Ultrasensitive Temperature Sensor With a Fully Liquid-Filled Photonic Crystal Fiber Mach–Zehnder Interferometer. *IEEE Sens. J.* **2014**, *14*, 167–170. [[CrossRef](#)]
65. Du, Y.; Qiao, X.; Rong, Q.; Yang, H.; Feng, D.; Wang, R.; Hu, M.; Feng, Z. A Miniature Fabry–Pérot Interferometer for High Temperature Measurement Using a Double-Core Photonic Crystal Fiber. *IEEE Sens. J.* **2014**, *14*, 1069–1073. [[CrossRef](#)]
66. Ding, W.-H.; Jiang, Y. Miniature Photonic Crystal Fiber Sensor for High-Temperature Measurement. *IEEE Sens. J.* **2014**, *14*, 786–789. [[CrossRef](#)]
67. Lopez-Aldaba, A.; Pinto, A.; Lopez-Amo, M.; Frazão, O.; Santos, J.; Baptista, J.; Baierl, H.; Auguste, J.-L.; Jamier, R.; Roy, P. Experimental and Numerical Characterization of a Hybrid Fabry–Pérot Cavity for Temperature Sensing. *Sensors* **2015**, *15*, 8042–8053. [[CrossRef](#)] [[PubMed](#)]
68. Scarcia, W.; Palma, G.; Falconi, M.; de Leonardis, F.; Passaro, V.; Prudenzano, F. Electromagnetic Modelling of Fiber Sensors for Low-Cost and High Sensitivity Temperature Monitoring. *Sensors* **2015**, *15*, 29855–29870. [[CrossRef](#)]
69. Pérez-Herrera, R.A.; André, R.M.; Silva, S.F.; Becker, M.; Schuster, K.; Kobelke, J.; Lopez-Amo, M.; Santos, J.L.; Frazão, O. Simultaneous measurement of strain and temperature based on clover microstructured fiber loop mirror. *Measurement* **2015**, *65*, 50–53. [[CrossRef](#)]
70. Revathi, S.; Inabathini, S.R.; Pal, J. Pressure and temperature sensor based on a dual core photonic quasi-crystal fiber. *Optik* **2015**, *126*, 3395–3399. [[CrossRef](#)]
71. Liu, Q.; Li, S.; Chen, H.; Li, J.; Fan, Z. High-sensitivity plasmonic temperature sensor based on photonic crystal fiber coated with nanoscale gold film. *Appl. Phys. Express* **2015**, *8*, 046701. [[CrossRef](#)]
72. Liu, Q.; Li, S.; Chen, H.; Fan, Z.; Li, J. Photonic Crystal Fiber Temperature Sensor Based on Coupling Between Liquid-Core Mode and Defect Mode. *IEEE Photonics J.* **2015**, *7*, 1–9. [[CrossRef](#)]
73. Wang, Q.; Du, C.; Zhang, J.; Lv, R.; Zhao, Y. Sensitivity-enhanced temperature sensor based on PDMS-coated long period fiber grating. *Opt. Commun.* **2016**, *377*, 89–93. [[CrossRef](#)]
74. Liu, C.; Wang, F.; Lv, J.; Sun, T.; Liu, Q.; Fu, C.; Mu, H.; Chu, P.K. A highly temperature-sensitive photonic crystal fiber based on surface plasmon resonance. *Opt. Commun.* **2016**, *359*, 378–382. [[CrossRef](#)]
75. Du, C.; Wang, Q.; Zhao, Y.; Li, J. Highly sensitive temperature sensor based on an isopropanol-filled photonic crystal fiber long period grating. *Opt. Fiber Technol.* **2017**, *34*, 12–15. [[CrossRef](#)]
76. Warren-Smith, S.C.; Nguyen, L.V.; Lang, C.; Ebendorff-Heidepriem, H.; Monroe, T.M. Temperature sensing up to 1300 °C using suspended-core microstructured optical fibers. *Opt. Express* **2016**, *24*, 3714. [[CrossRef](#)] [[PubMed](#)]
77. Nguyen, L.V.; Warren-Smith, S.C.; Ebendorff-Heidepriem, H.; Monroe, T.M. Interferometric high temperature sensor using suspended-core optical fibers. *Opt. Express* **2016**, *24*, 8967. [[CrossRef](#)]
78. Li, S.; Xia, L.; Chen, Z.; Yu, J.; Guan, H.; Lu, H.; Zhong, Y. Colloidal crystal cladding fiber based on side-polished fiber and its temperature sensing. *Opt. Quantum Electron.* **2017**, *49*, 66. [[CrossRef](#)]
79. Xu, Y.; Lu, P.; Chen, L.; Bao, X. Recent Developments in Micro-Structured Fiber Optic Sensors. *Fibers* **2017**, *5*, 3. [[CrossRef](#)]

80. Woyessa, G.; Fasano, A.; Markos, C.; Stefani, A.; Rasmussen, H.K.; Bang, O. Zeonex microstructured polymer optical fiber: Fabrication friendly fibers for high temperature and humidity insensitive Bragg grating sensing. *Opt. Mater. Express* **2017**, *7*, 286. [[CrossRef](#)]
81. Yang, X.; Lu, Y.; Liu, B.; Yao, J. Fiber Ring Laser Temperature Sensor Based on Liquid-Filled Photonic Crystal Fiber. *IEEE Sens. J.* **2017**, *17*, 6948–6952. [[CrossRef](#)]
82. Wang, Y.; Huang, Q.; Zhu, W.; Yang, M.; Lewis, E. Novel optical fiber SPR temperature sensor based on MMF-PCF-MMF structure and gold-PDMS film. *Opt. Express* **2018**, *26*, 1910. [[CrossRef](#)]
83. Gao, H.; Hu, H.; Zhao, Y.; Li, J.; Lei, M.; Zhang, Y. Highly-sensitive optical fiber temperature sensors based on PDMS/silica hybrid fiber structures. *Sens. Actuators A Phys.* **2018**, *284*, 22–27. [[CrossRef](#)]
84. Korganbayev, S.; Min, R.; Jelbuldina, M.; Hu, X.; Caucheteur, C.; Bang, O.; Ortega, B.; Marques, C.; Tosi, D. Thermal Profile Detection Through High-Sensitivity Fiber Optic Chirped Bragg Grating on Microstructured PMMA Fiber. *J. Light. Technol.* **2018**, *36*, 4723–4729. [[CrossRef](#)]
85. Zhao, Y.; Wu, Q.; Zhang, Y. Theoretical analysis of high-sensitive seawater temperature and salinity measurement based on C-type micro-structured fiber. *Sens. Actuators B Chem.* **2018**, *258*, 822–828. [[CrossRef](#)]
86. Lopez-Aldaba, A.; Auguste, J.-L.; Jamier, R.; Roy, P.; Lopez-Amo, M. Simultaneous Strain and Temperature Multipoint Sensor Based on Microstructured Optical Fiber. *J. Light. Technol.* **2018**, *36*, 910–916. [[CrossRef](#)]
87. Liu, Y.; Liu, X.; Ma, C.; Zhou, Y. Micro-structured optical fiber sensor for simultaneous measurement of temperature and refractive index. *Opt. Fiber Technol.* **2018**, *41*, 168–172. [[CrossRef](#)]
88. Zhao, L.; Han, H.; Lian, Y.; Luan, N.; Liu, J. Theoretical analysis of all-solid D-type photonic crystal fiber based plasmonic sensor for refractive index and temperature sensing. *Opt. Fiber Technol.* **2019**, *50*, 165–171. [[CrossRef](#)]
89. Su, H.; Zhang, Y.; Ma, K.; Zhao, Y.; Wang, J. High-temperature sensor based on suspended-core microstructured optical fiber. *Opt. Express* **2019**, *27*, 20156. [[CrossRef](#)] [[PubMed](#)]
90. Zhao, L.; Zhang, Y.; Chen, Y.; Wang, J. Composite cavity fiber tip Fabry-Perot interferometer for high temperature sensing. *Opt. Fiber Technol.* **2019**, *50*, 31–35. [[CrossRef](#)]
91. Ma, M.; Chen, H.; Zhang, W.; Li, S.; Jing, X. Temperature sensor based on a Sagnac interferometer using a liquid crystal-filled microstructured optical fiber. *Mater. Res. Express* **2019**, *6*, 085205. [[CrossRef](#)]
92. Zhao, J.; Zhao, Y.; Bai, L.; Zhang, Y. Sagnac Interferometer Temperature Sensor Based on Microstructured Optical Fiber Filled with Glycerin. *Sens. Actuators A Phys.* **2020**, *314*, 112245. [[CrossRef](#)]
93. Abdullah, H.; Mitu, S.A.; Ahmed, K. Magnetic Fluid-Injected Ring-Core-Based Micro-structured Optical Fiber for Temperature Sensing in Broad Wavelength Spectrum. *J. Electron. Mater.* **2020**, *49*, 4969–4976. [[CrossRef](#)]
94. Wang, M.; Chen, H.; Jing, X.; Li, S.; Ma, M.; Zhang, W.; Zhang, Y. Temperature sensor based on modes coupling effect in a liquid crystal-filled microstructured optical fiber. *Optik* **2020**, *219*, 165044. [[CrossRef](#)]
95. Zheng, B.; Yang, J.; Qi, F.; Wang, J.; Zhang, X.; Wang, P. Fabrication of Yb-doped silica micro-structured optical fibers from UV-curable nano-composites and their application in temperature sensing. *J. Non. Cryst. Solids* **2021**, *573*, 121129. [[CrossRef](#)]
96. Li, H.; Li, S.; Wang, S.; Zhang, S. Theoretical analysis of a microstructured fiber temperature sensor based on a Sagnac interferometer with a wide temperature measurement range. *Photonics Nanostructures—Fundam. Appl.* **2021**, *43*, 100858. [[CrossRef](#)]
97. Li, S.; Zhang, S.; Guo, Y.; Li, H.; Wang, Y.; Zhou, X.; Cheng, T. Experiment and Analysis of Temperature Sensing of Microstructured Fiber with Silver and PDMS Films. *Sensors* **2022**, *22*, 1447. [[CrossRef](#)]
98. Chen, X.; Yan, X.; Zhang, X.; Wang, F.; Suzuki, T.; Ohishi, Y.; Cheng, T. Highly sensitive nonlinear temperature sensor based on soliton self-frequency shift technique in a microstructured optical fiber. *Sens. Actuators A Phys.* **2022**, *334*, 113333. [[CrossRef](#)]
99. Liang, Y.; Zhang, H.; Huang, B.; Liu, B.; Lin, W.; Sun, J.; Wang, D. Ultrahigh-sensitivity temperature sensor based on resonance coupling in liquid-infiltrated side-hole microstructured optical fibers. *Sens. Actuators A Phys.* **2022**, *334*, 113358. [[CrossRef](#)]
100. Zhang, X.; Xu, Y.; Zhu, X.-S.; Shi, Y.-W. Surface plasmon resonance temperature sensor with tunable detection range based on a silver-coated multi-hole optical fiber. *Opt. Express* **2022**, *30*, 48091. [[CrossRef](#)] [[PubMed](#)]
101. Wildner, W.; Drummer, D. A Fiber Optic Temperature Sensor Based on the Combination of Two Materials With Different Thermo-Optic Coefficients. *IEEE Sens. J.* **2016**, *16*, 688–692. [[CrossRef](#)]
102. Pathak, A.K.; Chaudhary, D.K.; Singh, V.K. Broad range and highly sensitive optical pH sensor based on Hierarchical ZnO microflowers over tapered silica fiber. *Sens. Actuators A Phys.* **2018**. [[CrossRef](#)]
103. Khanikar, T.; Pathak, A.K.; Singh, V.K. Reflectance-based no core fiber sensor with enhanced Sensitivity for salinity detection. *Optik* **2018**, *159*. [[CrossRef](#)]
104. Pathak, A.K.; Singh, V.K. A wide range and highly sensitive optical fiber pH sensor using polyacrylamide hydrogel. *Opt. Fiber Technol.* **2017**, *39*. [[CrossRef](#)]
105. Wang, K.; Mizuno, Y.; Kishizawa, K.; Toyoda, Y.; Lee, H.; Ichige, K.; Kurz, W.; Dong, X.; Jakobi, M.; Koch, A.W. Temperature sensing based on multimode interference in polymer optical fibers: Sensitivity enhancement by PC-APC connections. *Jpn. J. Appl. Phys.* **2022**, *61*, 118001. [[CrossRef](#)]
106. Sun, X.; Zhang, L.; Zeng, L.; Hu, Y.; Duan, J. Micro-bending sensing based on single-mode fiber spliced multimode fiber Bragg grating structure. *Opt. Commun.* **2022**, *505*, 127513. [[CrossRef](#)]
107. Pathak, A.K.; Gangwar, R.K.; Priyadarshini, P.; Singh, V.K. A robust optical fiber sensor for the detection of petrol adulteration. *Optik* **2017**. [[CrossRef](#)]

108. Mallik, A.K.; Kumar, A.; Gupta, G.; Bhatnagar, A. Single mode fiber-optic temperature sensor fabricated using wet etching. In Proceedings of the 2012 International Conference on Fiber Optics and Photonics, Chennai, India, 9–12 December 2012.
109. Yang, R.; Yu, Y.-S.; Xue, Y.; Chen, C.; Wang, C.; Zhu, F.; Zhang, B.-L.; Chen, Q.-D.; Sun, H.-B. A Highly Sensitive Temperature Sensor Based on a Liquid-Sealed S-Tapered Fiber. *IEEE Photonics Technol. Lett.* **2013**, *25*, 829–832. [[CrossRef](#)]
110. Kumar, M.; Kumar, A.; Tripathi, S.M. A comparison of temperature sensing characteristics of SMS structures using step and graded index multimode fibers. *Opt. Commun.* **2014**, *312*, 222–226. [[CrossRef](#)]
111. Hao, X.; Tong, Z.; Zhang, W.; Cao, Y. A fiber laser temperature sensor based on SMF core-offset structure. *Opt. Commun.* **2015**, *335*, 78–81. [[CrossRef](#)]
112. Mohd Noor, M.Y.; Azmi, A.I.; Abdullah, A.S.; Mohd Supa'at, A.S.; Mohd Kassim, N.; Ibrahim, M.H.; Ngajikin, N.H. High Sensitivity of Balloon-Like Bent MMI Fiber Low-Temperature Sensor. *IEEE Photonics Technol. Lett.* **2015**, *27*, 1989–1992. [[CrossRef](#)]
113. Peng, X.; Cha, Y.; Zhang, H.; Li, Y.; Ye, J. Light intensity modulation temperature sensor based on U-shaped bent single-mode fiber. *Optik* **2017**, *130*, 813–817. [[CrossRef](#)]
114. Cai, L.; Liu, Y.; Hu, S.; Liu, Q. Optical fiber temperature sensor based on modal interference in multimode fiber lengthened by a short segment of polydimethylsiloxane. *Microw. Opt. Technol. Lett.* **2019**, *61*, 1656–1660. [[CrossRef](#)]
115. Huang, Q.; Wang, Y.; Zhu, W.; Lai, T.; Peng, J.; Lyu, D.; Guo, D.; Yuan, Y.; Lewis, E.; Yang, M. Graphene–Gold–Au@Ag NPs-PDMS Films Coated Fiber Optic for Refractive Index and Temperature Sensing. *IEEE Photonics Technol. Lett.* **2019**, *31*, 1205–1208. [[CrossRef](#)]
116. Li, X.; Tan, J.; Li, W.; Yang, C.; Tan, Q.; Feng, G. A high-sensitivity optical fiber temperature sensor with composite materials. *Opt. Fiber Technol.* **2022**, *68*, 102821. [[CrossRef](#)]
117. Wales, M.D.; Clark, P.; Thompson, K.; Wilson, Z.; Wilson, J.; Adams, C. Multicore fiber temperature sensor with fast response times. *OSA Contin.* **2018**, *1*, 764. [[CrossRef](#)]
118. Amorebieta, J.; Ortega-Gomez, A.; Fernández, R.; Antonio-Lopez, E.; Schülzgen, A.; Zubia, J.; Amezcua-Correa, R.; Durana, G.; Villatoro, J. Sensitivity-optimized strongly coupled multicore fiber-based thermometer. *Opt. Laser Technol.* **2022**, *145*, 107532. [[CrossRef](#)]
119. Cao, Z.; Zhang, Z.; Ji, X.; Shui, T.; Wang, R.; Yin, C.; Zhen, S.; Lu, L.; Yu, B. Strain-insensitive and high temperature fiber sensor based on a Mach–Zehnder modal interferometer. *Opt. Fiber Technol.* **2014**, *20*, 24–27. [[CrossRef](#)]
120. Chiavaioli, F.; Gouveia, C.; Jorge, P.; Baldini, F. Towards a Uniform Metrological Assessment of Grating-Based Optical Fiber Sensors: From Refractometers to Biosensors. *Biosensors* **2017**, *7*, 23. [[CrossRef](#)] [[PubMed](#)]
121. Hill, K.O.; Fujii, Y.; Johnson, D.C.; Kawasaki, B.S. Photosensitivity in optical fiber waveguides: Application to reflection filter fabrication. *Appl. Phys. Lett.* **1978**, *32*, 647–649. [[CrossRef](#)]
122. Rahman, B.M.A.; Viphavakit, C.; Chitree, R.; Ghosh, S.; Pathak, A.K.; Verma, S.; Sakda, N. Optical Fiber, Nanomaterial, and THz-Metasurface-Mediated Nano-Biosensors: A Review. *Biosensors* **2022**, *12*, 42. [[CrossRef](#)]
123. Chen, J.; Liu, B.; Zhang, H. Review of fiber Bragg grating sensor technology. *Front. Optoelectron. China* **2011**, *4*, 204–212. [[CrossRef](#)]
124. Zaynetdinov, M.; See, E.M.; Geist, B.; Ciovati, G.; Robinson, H.D.; Kochergin, V. A Fiber Bragg Grating Temperature Sensor for 2–400 K. *IEEE Sens. J.* **2015**, *15*, 1908–1912. [[CrossRef](#)]
125. Hsiao, T.-C.; Hsieh, T.-S.; Chen, Y.-C.; Huang, S.-C.; Chiang, C.-C. Metal-coated fiber Bragg grating for dynamic temperature sensor. *Optik* **2016**, *127*, 10740–10745. [[CrossRef](#)]
126. Dong, N.; Wang, S.; Jiang, L.; Jiang, Y.; Wang, P.; Zhang, L. Pressure and Temperature Sensor Based on Graphene Diaphragm and Fiber Bragg Gratings. *IEEE Photonics Technol. Lett.* **2018**, *30*, 431–434. [[CrossRef](#)]
127. Jasmi, F.; Azeman, N.H.; Bakar, A.A.A.; Zan, M.S.D.; Haji Badri, K.; Su'ait, M.S. Ionic Conductive Polyurethane-Graphene Nanocomposite for Performance Enhancement of Optical Fiber Bragg Grating Temperature Sensor. *IEEE Access* **2018**, *6*, 47355–47363. [[CrossRef](#)]
128. Cheng, P.; Wang, L.; Pan, Y.; Yan, H.; Gao, D.; Wang, J.; Zhang, H. Fiber Bragg grating temperature sensor of cladding with SrTiO<sub>3</sub> thin film by pulsed laser deposition. *Laser Phys.* **2019**, *29*, 025107. [[CrossRef](#)]
129. Gao, X.; Ning, T.; Zhang, C.; Xu, J.; Zheng, J.; Lin, H.; Li, J.; Pei, L.; You, H. A dual-parameter fiber sensor based on few-mode fiber and fiber Bragg grating for strain and temperature sensing. *Opt. Commun.* **2020**, *454*, 124441. [[CrossRef](#)]
130. Chen, Q.; Wang, D.N.; Gao, F. Simultaneous refractive index and temperature sensing based on a fiber surface waveguide and fiber Bragg gratings. *Opt. Lett.* **2021**, *46*, 1209. [[CrossRef](#)]
131. Esposito, F.; Campopiano, S.; Iadicicco, A. Miniaturized Strain-Free Fiber Bragg Grating Temperature Sensors. *IEEE Sens. J.* **2022**, *22*, 16898–16903. [[CrossRef](#)]
132. Fu, H.; Wang, S.; Chang, H.; You, Y. A high resolution and large range fiber Bragg grating temperature sensor with vortex beams. *Opt. Fiber Technol.* **2020**, *60*, 102369. [[CrossRef](#)]
133. Li, G.; Ji, L.; Li, G.; Su, J.; Wu, C. High-resolution and large-dynamic-range temperature sensor using fiber Bragg grating Fabry-Pérot cavity. *Opt. Express* **2021**, *29*, 18523. [[CrossRef](#)]
134. He, J.; Xu, X.; Du, B.; Xu, B.; Chen, R.; Wang, Y.; Liao, C.; Guo, J.; Wang, Y.; He, J. Stabilized Ultra-High-Temperature Sensors Based on Inert Gas-Sealed Sapphire Fiber Bragg Gratings. *ACS Appl. Mater. Interfaces* **2022**, *14*, 12359–12366. [[CrossRef](#)]
135. Guo, Q.; Zhang, Z.-D.; Zheng, Z.-M.; Pan, X.-P.; Chen, C.; Tian, Z.-N.; Chen, Q.-D.; Yu, Y.-S.; Sun, H.-B. Parallel-Integrated Sapphire Fiber Bragg Gratings Probe Sensor for High Temperature Sensing. *IEEE Sens. J.* **2022**, *22*, 5703–5708. [[CrossRef](#)]

136. Xu, B.; He, J.; Du, B.; Xiao, X.; Xu, X.; Fu, C.; He, J.; Liao, C.; Wang, Y. Femtosecond laser point-by-point inscription of an ultra-weak fiber Bragg grating array for distributed high-temperature sensing. *Opt. Express* **2021**, *29*, 32615. [[CrossRef](#)] [[PubMed](#)]
137. Sun, X.; Chang, Z.; Zeng, L.; Zhang, L.; Hu, Y.; Duan, J. Simultaneous vector bending and temperature sensing based on eccentric multi-mode fiber Bragg gratings. *Sens. Actuators A Phys.* **2021**, *331*, 112903. [[CrossRef](#)]
138. Hsu, C.-Y.; Chiang, C.-C.; Hsieh, T.-S.; Hsu, H.-C.; Tsai, L.; Hou, C.-H. Study of fiber Bragg gratings with TiN-coated for cryogenic temperature measurement. *Opt. Laser Technol.* **2021**, *136*, 106768. [[CrossRef](#)]
139. Ayupova, T.; Shaimerdenova, M.; Tosi, D. Shallow-Tapered Chirped Fiber Bragg Grating Sensors for Dual Refractive Index and Temperature Sensing. *Sensors* **2021**, *21*, 3635. [[CrossRef](#)]
140. Wang, Y.; Tao, J.; Yuan, W.; Lian, Z.; Ling, Q.; Chen, D.; Yu, Z.; Lu, C. Hollow Core Bragg Fiber Integrated With Regenerate Fiber Bragg Grating for Simultaneous High Temperature and gas Pressure Sensing. *J. Light. Technol.* **2021**, *39*, 5643–5649. [[CrossRef](#)]
141. Wang, H.; Gao, S.; Yue, X.; Cheng, X.; Liu, Q.; Min, R.; Qu, H.; Hu, X. Humidity-Sensitive PMMA Fiber Bragg Grating Sensor Probe for Soil Temperature and Moisture Measurement Based on Its Intrinsic Water Affinity. *Sensors* **2021**, *21*, 6946. [[CrossRef](#)]
142. Zhu, F.; Hao, X.; Zhang, Y.; Jia, P.; Su, J.; Wang, L.; Liu, L.; Li, X.; An, G. D-shaped optic fiber temperature and refractive index sensor assisted by tilted fiber bragg grating and PDMS film. *Sens. Actuators A Phys.* **2022**, *346*, 113870. [[CrossRef](#)]
143. Li, M.; Gong, Y.; Yin, J.; Li, W.; Shao, Y.; Cong, A.; Huang, G. Highly-sensitive and wide-range temperature sensor based on polymer-filled micro-cavity in fibre Bragg grating by temperature segmentation. *Optik* **2021**, *245*, 167707. [[CrossRef](#)]

**Disclaimer/Publisher’s Note:** The statements, opinions and data contained in all publications are solely those of the individual author(s) and contributor(s) and not of MDPI and/or the editor(s). MDPI and/or the editor(s) disclaim responsibility for any injury to people or property resulting from any ideas, methods, instructions or products referred to in the content.